[AMERICAN JOURNAL OF SCIENCE, 288, MAY 1988, P. 458-494]

DEVELOPMENT OF A CATACLASTIC FAULT ZONE IN AN ARCHEAN GRANITIC PLUTON OF THE SUPERIOR PROVINCE: STRUCTURAL, GEOCHEMICAL, AND GEOPHYSICAL CHARACTERISTICS

D. CHOUDARI KAMINENI,* ROBERT H. THIVIERGE, and DENVER STONE*

Atomic Energy of Canada Ltd., 601 Booth St., Ottawa, Ontario, K1A 0E8, Canada

ABSTRACT. A 4 m-wide fault zone was intersected by borehole ATK-6 at 1090 m true depth in the hornblende quartz monzodiorite rim of the Eye-Dashwa granite pluton near Atikokan, Ontario. The fault is composed of four major slip surfaces, up to 0.3 m wide, with a mean attitude of 182°/67°W, separated by a reticulate network of secondary fractures inclined at less than 25° to the slip surfaces. Sinistral strike-slip displacement seems to have occurred across the fault. The slip surfaces contain cataclastically deformed monzodiorite (quartz–hornblende–microcline–plagioclase ± sphene, apatite, zircon, titanomagnetite) and are dominated by a new mineral assemblage of hematite–albite–chlorite–epidote ± prehnite. The new assemblage formed, at least in part, by reconstruction of variably altered and recrystallized monzodiorite. Microprobe analyses reveal that primary edenitic hornblende and oligoclase (An_{15-18}) in the wall rock are increasingly converted within 10 to 12 m of the fault, first to ferrian magnesio-hornblende and sodic oligoclase (An_{10-13}), then to ferri-tremolitic hornblende or ferrian tremolite and albite (An_{1-5}), and ultimately to actinolite and albite (An_{0-2}). Epidote clasts and crenulated actinolite in the fault indicate that advanced alteration preceded some major movement. Chlorite, epidote, prehnite, and microcline are of relatively uniform composition within and outside the fault. Subsequent alteration of the fault rocks, resulting from (1) prolonged crystallization under late- to post-cataclastic conditions and (2) lower-temperature rock-water interactions around reactivated or open fractures, is marked to some extent by static prehnite, chlorite, and hematite growths, local development of barite + celestite, calcite + clay (kaolinite?) + chlorite, most potassic K-feldspar, and slight enrichments in the light rare-earth elements and U.

Faulting occurred during the late Archean or early Proterozoic under greenschist facies metamorphic conditions at estimated pressures of 2.5 to 3.5 kb and temperatures in the range of 325° to 400°C. Very low magnetic susceptibility values reflect breakdown of titanomagnetite in the fault zone relative to the monzodiorite while a weak but broad radioelement enrichment is shown by relatively high natural gamma values and modest increases in U concentrations. Low resistivity, fluid resistivity and acoustic velocity, and high spontaneous potential values show that the fault zone is electrically conduc-

* Present address: Applied Geoscience Branch, Whiteshell Nuclear Research Establishment, Pinawa, Manitoba R0E 1L0, Canada.

tive and suggest that it may be hydraulically permeable, compared to the wall rock.

INTRODUCTION AND SCOPE OF STUDY

Fault and fracture zones in Precambrian terrains, which represent zones of intense deformation between crustal blocks or in some cases major lithotectonic boundaries, are commonly expressed as arrays of topographic lineaments that form parallel features or anastomosing, mosaic-like patterns. Such zones are generally associated with past and/or present surface and subsurface aqueous flow. In recent years, detailed studies of fault and fracture zones have become imperative to the assessment of geotechnical problems and concept evaluation of nuclear fuel waste disposal in plutonic rock. However, the study of fault and fracture systems is commonly hindered by poor surface exposure as a result of their mechanical control on glaciation and various erosion processes. Many appear to underlie lineaments covered with glacial overburden and/or water. Consequently, the study of such features is strongly dependent on subsurface information derived from mining operations or diamond-drill core samples and borehole geophysical surveys.

Atomic Energy of Canada Limited has in the past six years conducted various geotechnical studies at a research area encompassing the Eye-Dashwa Lakes pluton, about 30 km northwest of Atikokan, northwestern Ontario, as part of the Canadian concept assessment for the geological disposal of nuclear fuel waste. Part of the research includes deep diamond-drilling of various plutonic rocks for structural, petrochemical, and geotechnical studies of fault and fracture characteristics within them.

This paper examines in detail a subsurface fault zone in the south-central margin of the Eye-Dashwa Lakes pluton. The fault zone is intersected at a depth of 1.1 km and may be expressed at the surface as one or two lineaments. The scope of this study involves examination of oriented core samples to investigate (1) the general structure and microstructures of the fault zone, (2) petrographic characteristics and mineral compositional variations, (3) whole-rock geochemical variations, (4) P-T conditions of cataclasis, and (5) geophysical characteristics of the fault zone.

GENERAL GEOLOGY AND STRUCTURE

The Eye-Dashwa Lakes pluton is a partially zoned elliptical body located in the Wabigoon subprovince of the Superior structural province near Atikokan, Ontario (fig. 1). The pluton occurs within the southeastern part of the Irene-Eltrut Lakes granite/gneiss complex (Schwerdtner, 1976; Schwerdtner and others, 1979) near the western margin of the Finlayson Lake and Steep Rock Lake greenstone belts (Shklanka, 1972; Fenwick, 1976; Stone, 1986). It is composed of two major intrusive centers of granodiorite to granite with a marginal phase

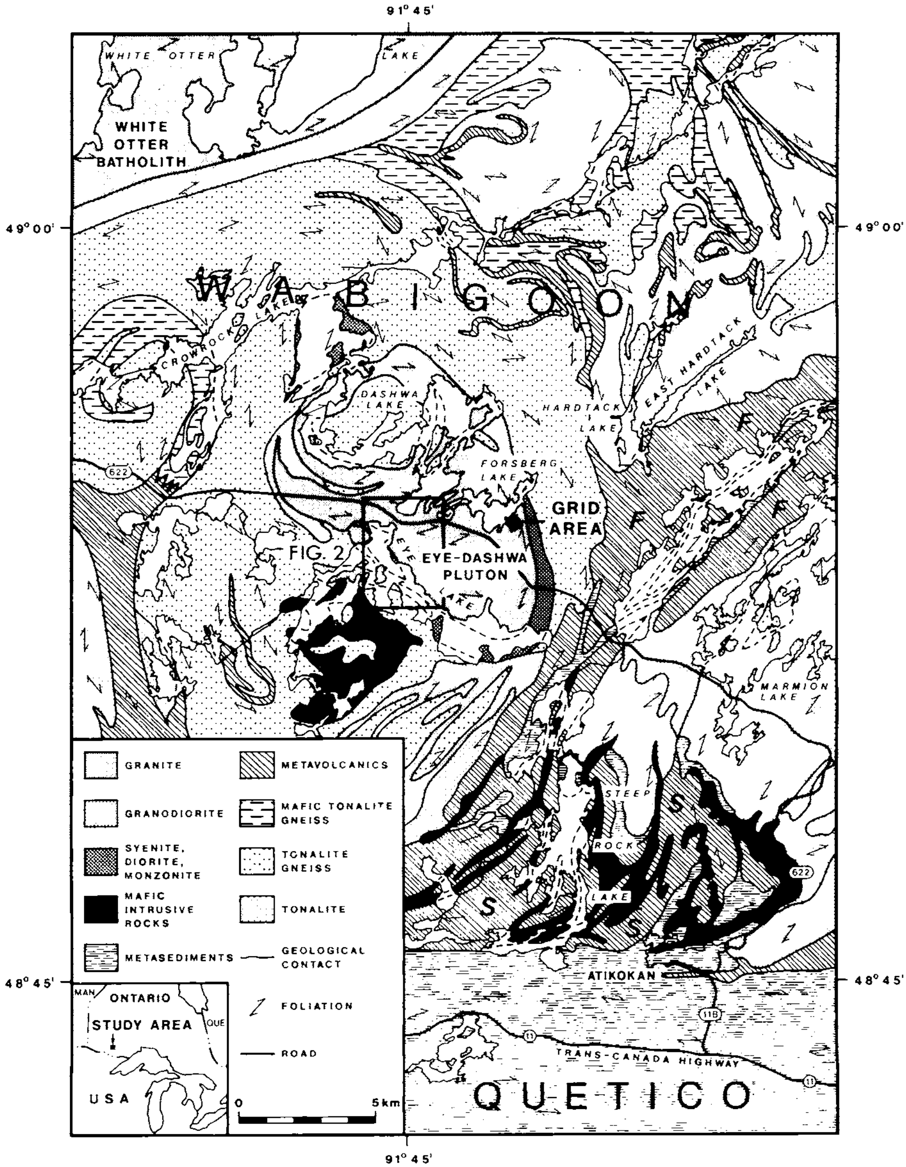

Fig. 1. Geological setting of Eye-Dashwa Lakes pluton, Atikokan area, Ontario (from Stone, 1986). F = Finlayson Lake greenstone belt; S = Steep Rock Lake greenstone belt. Outlined are Forsberg Lake research site (labelled "Grid Area") and area of figure 2.

of quartz monzodiorite to monzonite which partly rims the southeastern center of the pluton (Brown and others, 1980; Kamineni and Brown, 1981).[1] Monzodiorite also forms a discrete satellite stock northwest of the main pluton at Volcano Bay of Dashwa Lake. The pluton intrudes predominantly tonalitic gneiss, which forms elongate concordant enclaves in part outlining the intrusive centers, and a large oval roof pendant or pluton hood within the northwestern center. Xenoliths of metavolcanic amphibolite occur in the pluton's eastern margin. K-Ar dates on hornblende from the pluton give an age of 2658 ± 67 Ma implying that it was emplaced during the Kenoran orogeny (Kamineni and Stone, 1983).

The south-central margin of the Eye-Dashwa Lakes pluton (fig. 2) displays an inward zonation from foliated granodiorite and massive hornblende quartz monzodiorite/monzonite, which underlie much of Eye Lake, to massive to porphyritic granodiorite/monzonite. K-feldspar phenocrysts in the latter commonly define a weak flow fabric, which is generally subparallel to the pluton margin, but in this area trends easterly, slightly oblique to the pluton contact (fig. 1; see also fig. 1 of Brown and others, 1980). The location and surface trajectory of borehole ATK-6, which plunges steeply eastward and intersects a subsurface fault zone, are shown in figure 2, and an east-west vertical profile along the borehole trajectory is given in figure 3. The borehole is collared on granodiorite and intersects hornblende quartz monzodiorite from about 715 m to its bottom at 1201 m.[2] The fault zone cuts the monzodiorite phase between 1137 to 1144 m and contains a variety of cataclastic rocks (compare, Sibson, 1977; Wise and others, 1984).

Borehole ATK-6 lies in an intrablock domain characterized by eight weak fracture sets, low to intermediate bulk fracture density (Brown and Rey, 1985) and is devoid of significant geophysical anomalies (Sinha, Collett, and Bazinet, 1985).

Fault Zone

The fault zone in borehole ATK-6 occurs between 1137.5 to 1143.9 m; it is a steeply-dipping structure cutting massive, medium-grained leucocratic hornblende quartz monzodiorite which typifies the lower part of the borehole (fig. 3). The surrounding, relatively unaltered monzodiorite becomes highly fractured, brecciated, and cataclastically deformed in the fault zone, where altered monzodiorite predominates. These are the only rock types present in the vicinity of the fault, with the exception of a hornblende porphyry dike (1130.6–1131.2 m), an aplite dike (1132.6–.9 m), both in a hangingwall, and a feldspar porphyry dike (1147.3–1148.4 m) in the footwall.

[1] Terminology of plutonic rocks after Streckeisen (1976).
[2] All depths reported represent borehole length unless otherwise stated.

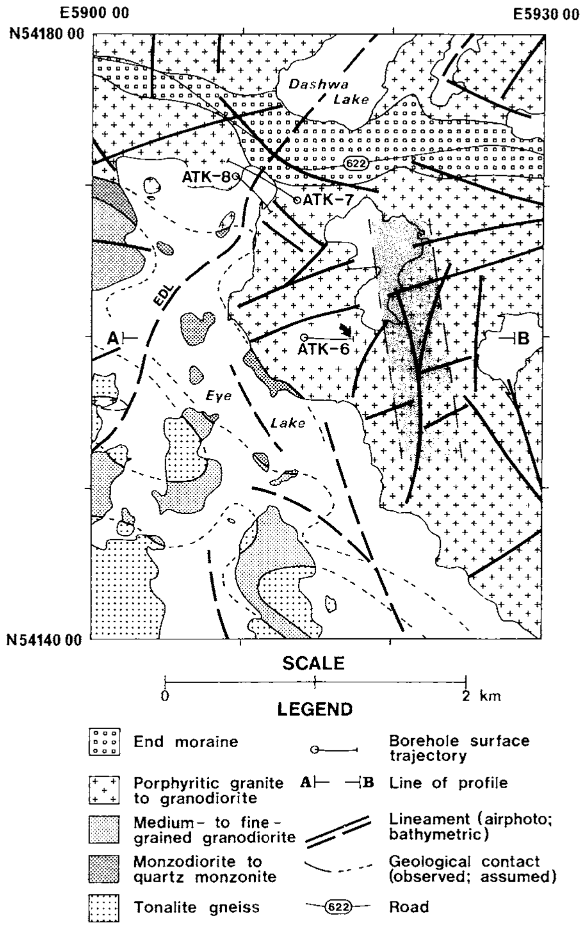

Fig. 2. General geology of south-central margin of Eye-Dashwa Lakes pluton, showing location and surface trajectory of borehole ATK-6. Shown also are the surface projection of deep fault intersection (arrow) and a band domain (light stipple) representing the 95 percent confidence limits of fault's surface exposure. A-B is line of profile in figure 3. Surface lineaments modified after Brown and others (1980). Bathymetric lineaments after lake bedrock topography and sediment isopach maps of Holloway (1985). EDL is Eye-Dashwa Lineament.

The fault zone is comprised of at least four discrete, major slip surfaces,[3] each between 3 to 30 cm thick, containing cataclasite and sporadic ultracataclasite (fig. 4), which are composed mainly of secondary epidote, chlorite, and hematite fillings. The slip surfaces occur at

[3] The term "slip surface" is used instead of "slip zone" to avoid confusion with the term "fault zone" and is used synonymously with a zone defining a relatively narrow (curvi) tabular body of intense cataclasis.

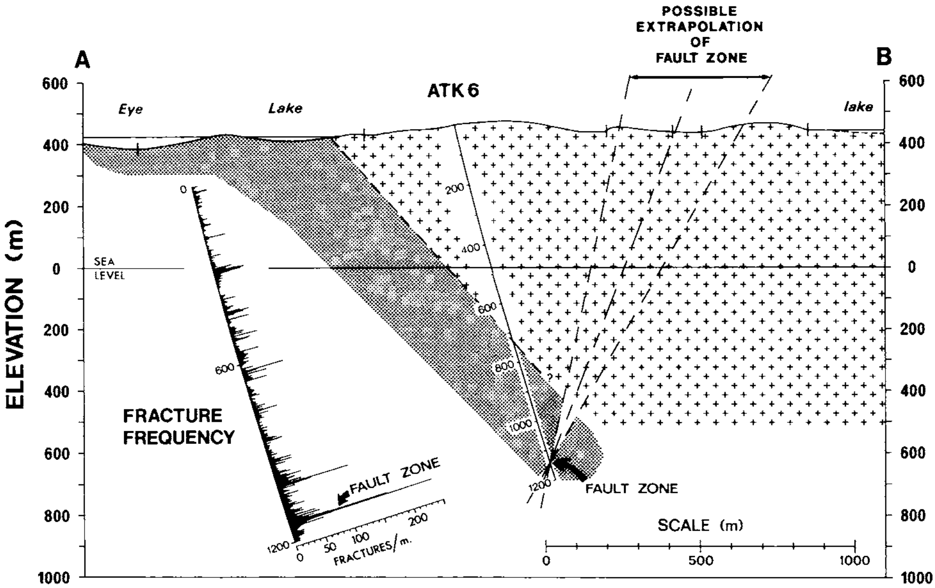

Fig. 3. Vertical west-east profile A-B showing the projection of the borehole and its deep intersection with the fault. Dashed surface extrapolation of the fault zone represents 95 percent confidence limits of an assumedly planar zone. Inset borehole profile shows fracture frequency per meter. Legend as in figure 2. Surface lineaments are expressed as short vertical bars.

1137.5 to 1137.7 m, 1140.1 to 1140.3 m, 1141.0 to 1141.5 m, and 1143.5 to 1142.8 m. They commonly exhibit a banded structure subparallel to their boundaries owing to domainal variation in color, mineralogy, and/or grain size, and a crude shape fabric defined by the dimensional alignment of fractured grains and elongate grain aggregates. Within the framework of the fault zone, the slip planes are interpreted as semi-continuous, roughly tabular zones of relatively large displacement. If the fault zone is considered to be bounded by the outer slip surfaces, then the two large internal slip surfaces are approximately symmetrically disposed about the center of the fault. Other possible slip surfaces of lesser significance and many fractures exhibiting displacement occur throughout the fault zone but contain little or no cataclastic fragments of the host rock, thinner fracture fillings, and less prominent internal planar structure. The slip surfaces have a mean true orientation of 172° (±9) strike and 67° (±9)W dip, which is considered to represent the local attitude of the fault zone (fig. 5A). Based on this attitude, the orthogonal thickness of the fault zone is about 4 m.

As shown in the fracture frequency histogram plotted along the borehole (fig. 3), the monzodiorite contains a low to medium fracture density away from the fault zone, except for local zones of more intense

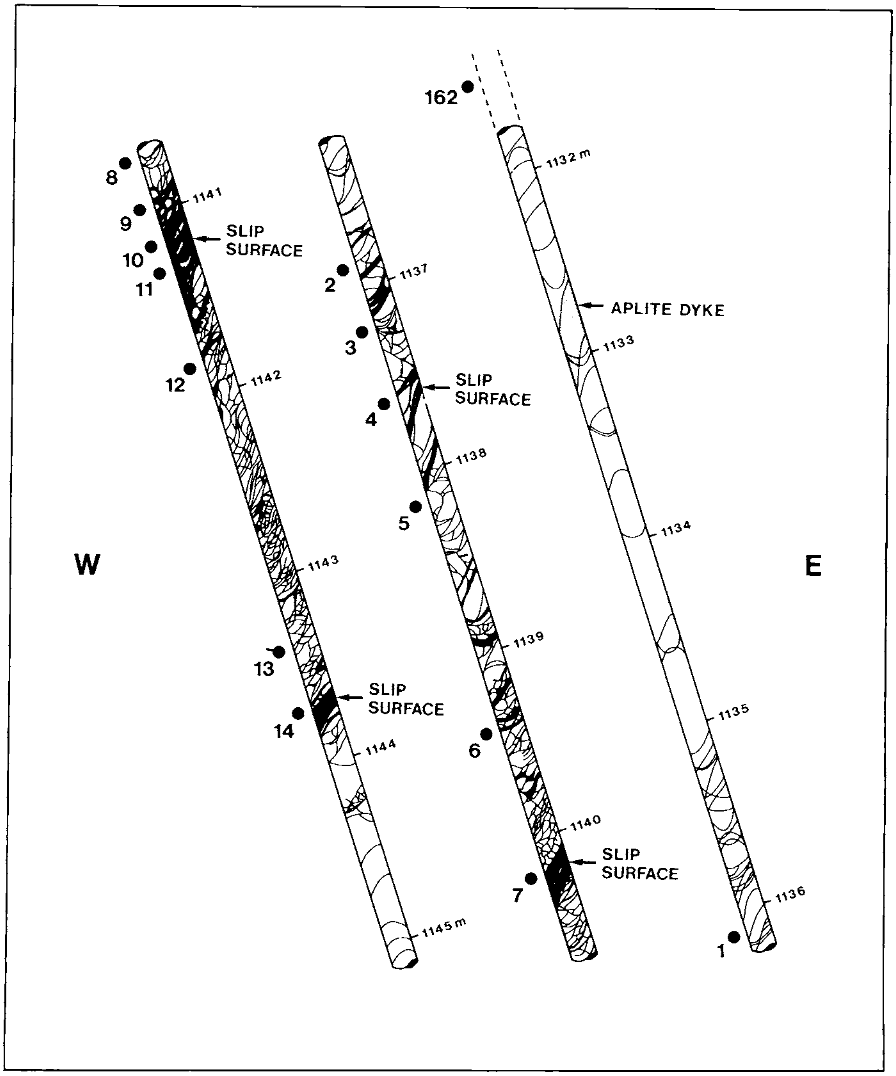

Fig. 4. Sketch of ATK-6 drill core showing major slip planes composed of cataclasite to ultracataclasite (black) and fractures (thin lines) within the fault zone, and sample locations (1–14). Core axis plunges 72° easterly, and view is northward. Borehole length in meters.

fracturing. Fracture frequency rises progressively but asymmetrically into the fault, being more abrupt from the footwall than from the hangingwall. Number of fractures increases rapidly in a 10 m borehole interval below 1135.0 m, preceding the upper bounding slip surface of the fault, and above 1143.9 m, adjacent to the lower bounding slip surface.

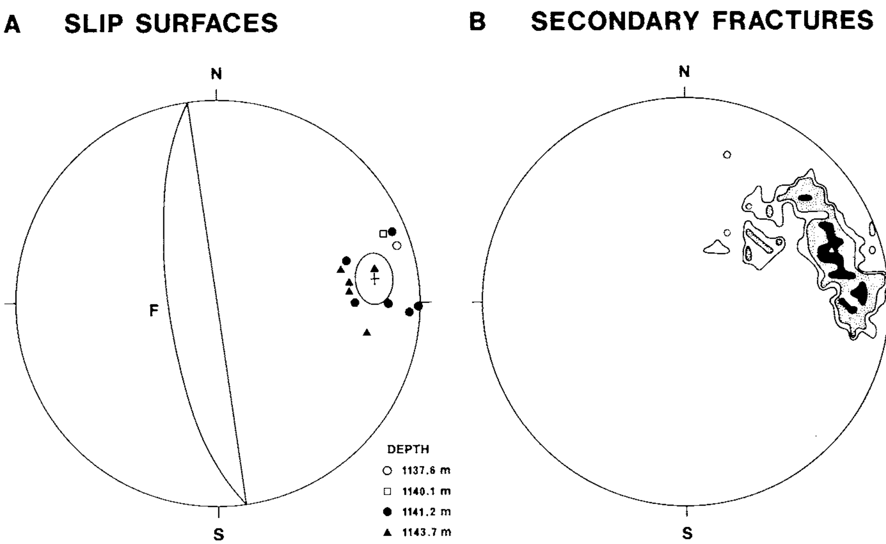

Fig. 5. Lower hemisphere equal-area stereoplots of orientations within the fault zone. (A) poles to planar features (n = 13) within the four slip surfaces. Cross and circled areas represent the mean pole orientation and 95 percent confidence limits, respectively, for the fault plane, F. (B) contoured pole densities for fracture orientations in the three fracture zones between the slip surfaces (contours at 3, 4, and 6 percent; a maximum density of 8 percent shown by open triangle; n = 140).

Within the fault zone (that is, between the bounding slip surfaces) the monzodiorite is variably altered, fractured, and comminuted and is mainly comprised of breccia with subordinate protocataclasite. The degree of brecciation is weak to moderate in the upper part of the zone (between 1136.9–1139.8 m) where slip surfaces are relatively thin, and more intense in the lower part (1139.8–1143.7 m) where slip surfaces are thicker (fig. 4). Many thin, secondary fractures within the fault are individually discontinuous on the core surface, tend to curve and splay, and form the breccia framework between the slip surfaces. These secondary fractures, both with and without apparent displacement, are generally inclined at less than 25° to the mean slip surface (fig. 5B). The asymmetry between the slip surfaces and many of the secondary fractures is suggestive of largely strike-slip displacement of uncertain sense. However, the observed offsets along similarly oriented faults at the surface, as in the "grid area" of figure 1 (Stone, 1983, 1985), generally indicate sinistral shear sense.

Surface extrapolation.—Although orientations observed within the fault zone are common in the region of the Eye-Dashwa Lakes pluton and correspond well with lineament trends (Brown and others, 1980), they are poorly represented by fracture orientations at the surface surrounding the borehole (Brown and Rey, 1985). On the assumption that the fault zone is a semi-infinite planar structure of tabular or disc-like form, its projection to the surface is represented by a band domain 400 m wide with 95 percent confidence limits for exposure (figs. 2 and 3). From inspection of airphotographs, two coalescing lineaments occur within this band domain, each or both of which may be surface expressions of the subsurface fault zone. Unfortunately, bedrock is not exposed along or close to these lineaments, and no anomalies in fracture intensity or orientation are observed in their vicinity at the surface (Brown and Rey, 1985). Another northerly-trending lineament, which also constitutes a likely candidate for surface extrapolation of the fault zone, occurs immediately west of the band domain at a cliff face, controlled by steeply (80°–85°) westward-dipping fractures, and, like the subsurface fault, corresponds to a well-developed magnetic susceptibility low relative to the surrounding rock. Subsurface correlation in this case allows for curvature of the fault zone and a slight shallowing of attitude (about 20°) with depth.

PETROGRAPHY AND MICROSTRUCTURES

Isotropic Quartz Monzodiorite

Relatively unaltered and unfractured hornblende quartz monzodiorite is similar above and below the fault zone and may be considered structurally isotropic with respect to highly fractured rocks of the fault zone. From petrographic examination of thin sections (fig. 6A) the rock is massive, medium-grained, and inequigranular, with grain size generally ranging between 0.2 to 2.0 mm, and averaging approx 0.5 to 0.8 mm. The rock is leucocratic, with color index between 5 to 15 percent, and possesses hypidiomorphic-granular texture. Primary mineralogy is dominated by plagioclase (30–40 percent), microcline (30–35 percent), hornblende (5–15 percent), which tend to form coarser grains, and quartz (5–15 percent), which is interstitial and generally fine-grained. Primary biotite is locally associated with amphibole, which occurs as individual crystals or in small dispersed groups of crystals. Accessory minerals account for up to 5 percent of the rock and include subhedral to euhedral sphene, apatite, titanomagnetite, and rarer zircon. Hornblende displays blue to light green pleochroism and has irregular or ragged outlines but is locally subhedral, rarely euhedral, and poikilitically or partially encloses these accessory minerals (fig. 6A), as well as plagioclase and microcline.

Minerals of secondary origin include epidote, chlorite, carbonate, white mica, prehnite, clinozoisite, and hematite. These are generally finer-grained (<0.5 mm) and constitute less than 2 to 3 percent of the wallrock monzodiorite. Epidote and chlorite are commonest as marginal and internal alterations of hornblende but also occur within feldspar. Brown chlorite commonly replaces hornblende internally in the form of branching ribbon-like growths or rounded patches. Carbonate, white mica, and prehnite occur as fine-grained alteration products within plagioclase.

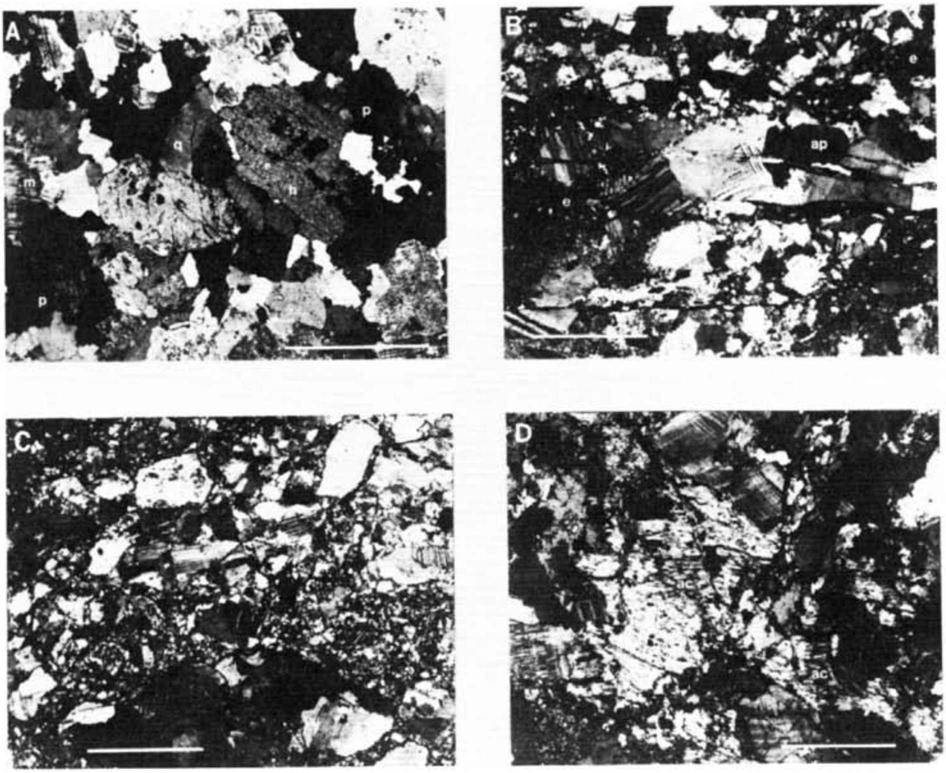

Fig. 6(A) Microphotograph of relatively unaltered hornblende quartz monzodiorite wallrock (h = hornblende, p = plagioclase, m = microcline, q = quartz). Sample ATK-6-166, cross-polarized light. Scale bar is 2.0 mm (GSC 203555-X).

(B) Microphotograph of altered hornblende quartz monzodiorite showing development of secondary minerals and transgranular fracturing in protocataclasite (e = epidote, ap = apatite). Sample ATK-6-3, cross-polarized light. Scale bar is 1.0 mm (GSC 203671-Y).

(C) Microphotograph of mechanically disrupted feldspar in cataclasite. Sample ATK-6-14, cross-polarized light. Scale bar is 1.0 mm (GSC 203555-Y).

(D) Microphotograph of crenulated and sheared actinolite (ac) clasts in cataclasite. Sample ATK-6-13, cross-polarized light. Scale bar is 1.0 mm (GSC 203671-X).

Altered Quartz Monzodiorite of the Fault Zone

Cataclastic rocks of the fault zone display mechanically disrupted mineral (feldspar, quartz, hornblende, sphene, apatite, zircon) and rock fragments in a fine- to extremely fine-grained neocrystallized matrix dominated by epidote, chlorite, and albite. The fault zone is characterized by brecciated, altered monzodiorite and protocataclasite (for example, fig. 6B,D). However, cataclasite and ultracataclasite are well developed, particularly within the slip surfaces (figs. 6C, 7A–C).

Based on the volume of porphyroclastic minerals and aggregates, and on matrix grain size, varieties of cataclastic rocks are gradational

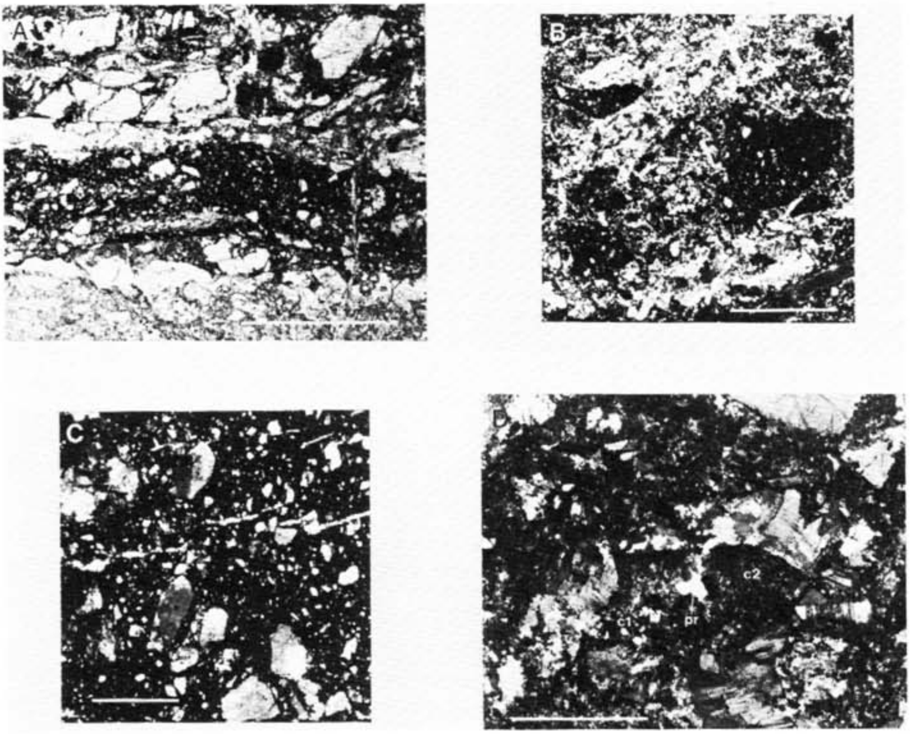

Fig. 7(A) Microphotograph of discontinuous banded structure developed locally in cataclasite slip planes. Sample ATK-6-9, plane-polarized light. Scale bar is 2.0 mm (GSC 202824-N).

(B) Microphotograph of dark epidote-rich cataclasite/ultracataclasite fragments enclosed within plagioclase-rich cataclasite matrix. Sample ATK-6-7, cross-polarized light. Scale bar is 3.0 mm (GSC 203671-T).

(C) Microphotograph of irregular albite veinlets intruding cataclasite and themselves displaced by epidote- and chlorite-filled fractures. Sample ATK-6-7, cross-polarized light. Scale bar is 1.0 mm (GSC 204220-T).

(D) Microphotograph of highly altered monzodiorite showing prehnite (pr) development in plagioclase and in the core a corona-like growth, surrounded by a pale chlorite (cl) plus iron oxide which grades outward to a darker chlorite (c2). Sample ATK-6-12, cross-polarized light. Scale bar is 1.0 mm (GSC 203555-W).

over distances commonly less than 1.0 cm. While no classification of cataclastic rocks based strictly on grain size is in geological usage (compare Higgins, 1971; Sibson, 1977), in general, the grain size of matrix and of porphyroclasts decreases with progressive intensity of cataclasis. Typical matrix grain sizes of cataclasite and ultracataclasite in the ATK-6 fault zone range between 5 to 50 mm, whereas porphyroclasts within them may be of equivalent dimension as well as much coarser, up to 250 to 350 mm long.

The secondary mineralogy of relatively unaltered, isotropic wall rock and the dominant mineralogy of cataclastic rocks in the fault zone are similar but vary significantly in proportion. Epidote and chlorite, present in minor amounts in the wall rock, become major constituents of the fault zone (figs. 6B–D, 7B–D): they form widespread alteration products within the monzodiorite breccia fragments as well as the bulk of the fracture-filling mineral assemblage, with variable combinations of hematite, specular hematite, and albite. While most slip surfaces within the fault zone contain much epidote and chlorite, the lower slip surface and fractures around it are, in contrast, dominated by hematite-rich fillings.

Feldspars, quartz, and amphibole are present throughout, but their amounts decrease significantly within the fault zone, where they form disrupted or cataclastic fragments with reduced grain size (fig. 6B–D). The primary hornblende, oligoclase, and microcline display systematic compositional variation reflecting alteration to actinolite, albite, and more postassic K-feldspar, respectively, within the fault zone. Titanomagnetite reacts to hematite, the dominant iron oxide phase within the fault zone resulting in an extreme lowering of magnetic susceptibility values in the fault zone. Local primary biotite is converted to chlorite. Accessory primary apatite and zircon show no significant alteration into the fault, although they are mechanically altered in form (for example, fig. 6B). Sphene crystals locally show thin rims or patchy alteration products of hydrous iron-titanium oxides. Extreme alteration, involving complete replacement of sphene such as is observed in an open fracture environment (Kamineni, 1986a), occurs locally but is restricted to highly altered sections of the lower half of the fault zone. These sections appear to have suffered prolonged alteration subsequent to the main period of cataclasis. The instability of sphene may be due to low activity of CO_2, that is, less than 0.5, in the alteration fluid (compare, Hunt and Kerrick, 1977).

Actinolite is commonly disrupted or crenulated (fig. 6D) and forms porphyroclasts in the fault zone. Epidote also occurs as porphyroclasts that are relatively coarser-grained than epidote of the cataclastic matrix and appears to be reworked secondary epidote of the host rock. These observations attest to the fact that advanced recrystallization and alteration of monzodiorite had occurred prior to at least some of the major cataclasis observed within the fault. Moreover, the presence of subrounded to subangular fragments of finer-grained ultracataclasite within cataclasite (for example, fig. 7B) infers a protracted history of fault deformation involving intermittent cataclasis and induration, possibly related to stick-slip motions.

Cataclastic mechanical processes involving transgranular and intragranular microfracturing, grain boundary sliding, and rigid body motions appear to be responsible for most of the deformation in the fault zone. Since the alteration of the host rock primary minerals is restricted to the vicinity of the fault zone and the alteration products are widespread and deformed within it, the alteration is related to grain boundary fluids and was enhanced by perturbations in the stress configuration caused by early fault evolution. For example, Simpson (1986) suggests that fluid-assisted alteration and hydrolytic weakening of host rock minerals, as well as the introduction of new mineral species in brittle-to ductile fault zones, may contribute to early fracturing and even the localization of plastic deformation.

In the ATK-6 fault zone, plastic deformation is evident on a limited microscopic scale to kinking and warping of twinning in plagioclase and microcline, crenulation of actinolite porphyroclasts, and possibly in the development of planar zones of subgrain structure in quartz and feldspars along the traces of microfractures. The compositional banding and mineral fabrics developed in cataclasite and fault gouge (House and Gray, 1982; Chester, Friedman, and Logan, 1985) may result purely from brittle, low-temperature processes as shown for natural and experimental structures (Chester, Friedman, and Logan, 1985), or by localized changes to crystal plastic deformation in brittle-to-ductile shear zones generally assisted by metamorphic reactions involving pressure solution (for example, Mitra, 1984; Stel, 1986). Sibson (1986) suggests that such foliated cataclasites are more likely indicative of relatively steady shearing flow in aseismic regimes (compare Sibson, 1977).

The banded structures of the slip surfaces, such as the elongation of porphyroclast trains (fig. 7A), likely relate entirely to cataclastic mechanisms of grain boundary sliding and attrition by sidewall fracturing and spalling, although such structure defined by grain size and color variation may result from some combination of degree of mineral comminution and/or neomineralization of secondary epidote. No aligned mineral growth fabrics or mineral flattening or fluxion-like structures are evident in the ATK-6 slip surfaces, suggesting that cataclastic flow was not achieved.

Late- to Post-Cataclastic Features

Numerous thin, irregular, and mutually intersecting albite/quartz veinlets commonly cut the cataclastic and ultracataclastic rocks but are in turn offset by thin epidote-bearing fractures which fade into the surrounding host rock (fig. 7C). The irregular and curved form of these veins, their reticulate and mutually intersecting relationships suggest either that the host rock had achieved some degree of consolidation, or hydraulic fracturing had occurred under conditions where $P_{fluid} > \sigma + T_o$, where σ is the least principal confining stress, and T_o is the tensile strength of the rock. Some major movements and epidote and chlorite crystallization persisted during and/or followed formation of the albite/quartz veinlets. These features indicate a late or post cataclasis brittle environment in which the activity of the pore fluids was such that first albite/quartz and then again epidote was stable. The veinlets themselves host a secondary chlorite after albite suggesting they were contiguous with continued chlorite formation during or after the later stages of fault activity.

At least two later mineral assemblages are associated with extreme alteration resulting from (A) prolonged crystallization under late- to post-cataclasis static conditions and (B) later open-fracture controlled rock-water interaction. The former assemblage contains prehnite, calcite, and chlorite and is locally well developed within cataclasite (samples 7 and 9). The abundant development of prehnite and calcite is notable in that these are much rarer in other cataclasite samples of the fault zone. Prehnite, which is found as an idioblastic alteration product within albite, is also developed within the cores of alteration coronas in chloritic aggregates, surrounded first by a weakly birefringent gray (magnesian?) chlorite or serpentine, associated with iron oxide and epidote, which grades outward to a brown birefringent chlorite (fig. 7D). The brown chlorite in these samples commonly forms isolated and well-developed ovoid aggregates, presumably after amphibole and/or iron oxide, with rosette-like or 'blocky' internal growth patterns. These textures suggest progressive evolution of the initial fault-related alteration mineralogy into conditions of local static growth. Well-developed brown chlorite aggregates suggest prolonged and/or enhanced crystallization of this mineral, as is similarly reflected within other cataclasites by late chlorite replacement of vein albite. It is likely that the corona-like growths developed during and/or after periods of cataclasis and reflect, to some degree, small-scale compositional variations relating to changing physical conditions, such as of crustal levels. A knowledge of the development of such corona-like growth types in low-grade brittle deformational regimes may yield significant information regarding crustal readjustments (for example, uplift) in lowgrade terrains similar to that derived from complex coronites in mafic rocks from high-grade gneissic terrains (Griffin and Heier, 1973).

The second mineral assemblage appears to relate to rock-water interaction in an "open-fracture" environment and contains calcite, chlorite, and clay (kaolinite?), with local associated barite and celestite (identified by scanning electron microscope). Fractures that are presently open and possibly open to groundwater flow, as detected by borehole acoustic televiewer, occur at 1139.19 and 1141.34 m, respectively (J.S.O. Lau, unpub. borehole data, personal commun, 1985), in close proximity to samples displaying this assemblage in thin section (samples 9 and 12). Calcite, kaolinite, and brown chlorite are also present in this "open fracture" environment.

It is apparent that the development of chlorite has occurred during various periods and under various conditions within the fault zone.

MINERAL COMPOSITIONS

Feldspars.—Both plagioclase and K-feldspar show distinct compositional variation between the relatively pristine quartz monzodiorite and its altered, cataclastic counter part. This variation is most pronounced in plagioclase (table 1) and spans an An content range of about 20 percent in the oligoclase-albite field. In the wall rock away from the fault zone, the plagioclase is a calcic oligoclase (An_{15-28}), which is believed to be a primary or near-primary composition (fig. 8). In the altered, cataclastic

TABLE 1

Microprobe analyses of plagioclase

	WALLROCK		FAULT ZONE										WALLROCK			
Sample No:	161	162	1	2	3	4	6	7	8	10	12	14	163	164	165	166
SiO_2	64.40	64.47	68.48	68.45	68.82	68.35	68.57	68.19	69.23	67.59	68.67	68.21	66.26	66.11	64.48	65.11
Al_2O_3	22.43	22.30	19.77	20.15	19.67	19.08	19.35	19.27	19.47	19.79	19.75	19.33	20.26	21.53	22.18	21.73
FeO*	0.17	0.11	0.02	0.01	0.03	0.13	0.04	0.15	0.18	0.07	0.07	0.04	0.06	0.08	0.13	0.09
CaO	3.45	2.71	0.33	0.05	0.00	0.16	0.17	0.22	0.14	0.37	0.02	0.17	1.28	2.23	3.76	3.35
Na_2O	9.86	10.32	12.03	11.81	12.08	11.57	11.18	11.46	11.49	11.50	11.82	12.11	11.46	10.56	9.55	10.56
K_2O	0.21	0.16	0.11	0.21	0.13	0.12	0.13	0.10	0.11	0.40	0.10	0.13	0.34	0.14	0.45	0.14
Total	100.52	100.07	100.74	100.68	100.69	99.41	99.44	99.29	100.64	99.72	100.43	99.99	99.66	100.65	100.55	100.98
Structural Formulae (based on 32 oxygens)																
Si	11.342	11.645	11.929	12.016	12.061	12.012	12.033	12.021	12.019	11.897	11.950	12.021	11.762	11.536	11.364	11.52
Al	4.655	4.638	4.062	4.015	4.053	3.998	4.002	4.013	3.976	4.118	4.054	4.002	4.225	4.468	4.579	4.47
Ca	0.648	0.516	0.066	0.010	0.000	0.032	0.032	0.022	0.021	0.074	0.000	0.033	0.201	0.419	0.705	0.65
Na	3.361	3.531	4.041	3.886	3.939	3.987	3.821	3.947	3.893	3.919	3.987	4.021	3.910	3.576	3.241	3.47
K	0.042	0.038	0.021	0.041	0.021	0.032	0.032	0.021	0.021	0.085	0.022	0.032	0.043	0.031	0.105	0.03
Molecular Proportions (%)																
An	16.2	12.5	1.5	0.2	0.0	0.0	0.8	0.6	0.5	1.9	0.0	0.8	4.9	10.4	17.4	15.4
Ab	82.8	86.5	98.0	98.8	99.4	99.5	98.4	98.9	99.0	96.0	99.5	98.4	94.1	88.8	80.0	83.8
Or	1.0	1.0	0.5	1.0	0.6	0.5	0.8	0.5	0.5	2.1	0.5	0.8	1.0	0.8	2.6	0.8

* Total Fe as FeO.

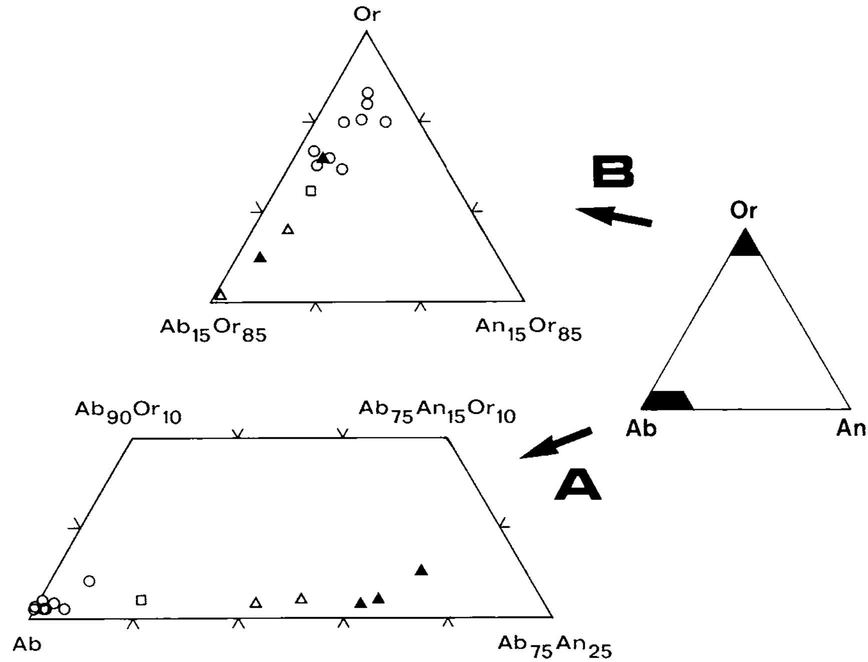

Fig. 8. Ab-An-Or ternary diagram showing compositional variation of (A) plagioclase and (B) microcline across the fault zone. Solid triangles relatively unaltered feldspars; open triangles weakly altered feldspars; square moderately altered feldspars; circles highly altered feldspars.

zone it becomes almost pure albite (An_{0-5}) (fig. 8A). No plagioclase zonation or rimming is evident petrographically. Plagioclase retains polysynthetic twinning through all compositional stages, but this may be kinked or disrupted by protracted mechanical activity within the fault zone after alteration.

Microcline is microperthitic and displays a modest Or content variation from Or_{92-98}, being generally more potassic in the fault zone (table 2). Their compositional characteristics are illustrated in fig. 8B. The most potassic microcline analyzed comes from the lower, hematite-rich slip zone.

Hornblende.—Hornblende, which is ubiquitous throughout the host quartz monzodiorite, not only becomes diminished in relative proportion but also shows dramatic compositional variation in relation to the fault zone (table 3). The hornblende is categorized as edenite or ferrain edenite in the primary quartz monzodiorite away from the fault (based on the IMA amphibole classification (Leake, 1978: Rock and Leake, 1984)). This composition is converted to ferrain magnesio-hornblende, ferri-tremolitic hornblende, or ferrain tremolite in regions

TABLE 2

Microprobe analyses of microcline

	WALLROCK		FAULT ZONE									WALLROCK			
Sample No:	161	162	1	2	3	4	5	6	7	8	14	163	164	165	166
SiO_2	63.93	65.23	64.33	64.64	65.24	64.57	65.94	64.44	64.57	64.58	64.41	64.90	64.65	63.95	64.89
Al_2O_3	18.69	18.64	18.55	18.91	18.69	18.77	19.22	18.86	18.69	18.83	18.85	18.97	19.29	18.91	18.89
FeO*	0.06	0.02	0.01	0.11	0.08	0.04	0.01	0.15	0.22	0.09	0.00	0.03	0.07	0.03	0.08
CaO	0.29	0.03	0.27	0.35	0.29	0.53	0.28	0.17	0.40	0.46	0.31	0.33	0.33	0.25	0.28
Na_2O	0.63	1.52	0.68	0.60	0.39	0.57	0.33	0.64	0.23	0.32	0.19	0.81	1.02	1.31	0.62
K_2O	15.74	15.28	15.80	15.74	15.90	16.00	14.52	15.86	15.84	16.34	15.70	15.80	14.69	14.91	15.61
Total	99.34	100.72	99.64	100.35	100.59	100.48	100.30	100.12	99.93	100.62	99.46	100.84	100.05	99.36	100.37
Structural Formulae (based on 32 oxygens)															
Si	11.898	11.902	11.933	11.911	11.977	11.902	12.003	11.905	11.953	11.899	11.957	11.893	11.882	11.913	11.933
Al	4.111	4.052	4.057	4.107	4.047	4.080	4.125	4.105	4.081	4.081	4.051	4.101	4.179	4.154	4.099
Ca	0.056	0.010	0.053	0.066	0.055	0.105	0.055	0.033	0.078	0.088	0.069	0.068	0.065	0.045	0.055
Na	0.224	0.605	0.245	0.210	0.143	0.205	0.120	0.233	0.078	0.111	0.069	0.292	0.362	0.458	0.221
K	3.741	3.609	3.741	3.697	3.728	3.764	3.370	3.743	3.736	3.837	3.832	3.722	3.443	3.526	3.657
Molecular Proportions(%)															
An	1.4	0.3	1.3	1.7	1.4	2.6	1.6	0.8	2.0	2.2	1.7	1.7	1.7	1.1	1.4
Ab	5.6	14.3	6.1	5.3	3.6	5.0	3.4	5.8	2.0	2.7	1.7	7.1	9.3	11.4	5.6
Or	93.0	85.4	92.6	93.0	95.0	92.4	95.0	93.4	96.0	95.1	96.6	91.2	89.0	87.5	93.0

* Total Fe as FeO.

immediately bounding the fault. Actinolite prevails within cataclasites in the fault zone and represents the microstructural-compositional end-member. These compositional variations reflect an obvious relative depletion in iron and enrichment in magnesium and calcium in amphiboles of the fault zone. In addition, figure 9 shows that primary and relatively unaltered hornblendes, plotting close to an ideal edenite composition, become nearly pure actinolite.

Sphene.—Sphene is ubiquitous in the cataclasite samples and occurs as relict crystals within highly altered amphibole crystals and as isolated crystals in the epidote-rich matrix. Sphene compositions from wall rock and cataclasite samples are chemically indistinguishable (table 4). This suggests that, unlike other minerals, sphene composition is virtually unaffected by mechanical or chemical alteration processes related to cataclasis.

Epidote.—Epidote is a ubiquitous alteration product in the wall rock and is the main secondary constituent of the fault zone breccia and cataclasite. Chemical analyses from both are presented in table 5. Epidote composition within the wall rock is inhomogeneous and shows a compositional range evident at the grain scale that is related to the various minerals it replaces. For example, as shown in figure 10, within a single thin section (see sample 162, table 5), epidote rimming titanomagnetite is extremely rich in iron, whereas epidote replacing plagioclase is characterized by much lower iron and higher aluminum contents, and epidote after amphibole is of intermediate composition. These compositional variations are presumably due to local variations in fO_2, which may profoundly influence epidote composition (Holdaway, 1972). However, epidote composition within breccia and cataclasite of the fault zone is relatively uniform, with a member of intermediate iron content predominating (fig. 10). The homogeneity of epidote composition within the cataclasites and breccia thus implies a uniformity of fO_2 in the fault zone environment.

The calcium content of epidote shows a general decreasing trend toward the center of the fault zone. All epidotes within the fault contain less than 22 wt percent CaO, slightly lower than epidote after titanomagnetite and much lower than other epidotes after plagioclase and hornblende (see table 5).

Chlorite.—Chlorite occurs as a minor alteration product of hornblende and to a lesser extent of feldspar and biotite within the wall rock. However, it becomes one of the major constituents in the fault zone. Compositionally, chlorite analyses from both wall rock and cataclasite samples (table 6) fall in the pycnochlorite field of Hey (1954). However, as shown in figure 11, subtle composition differences are apparent such that chlorites in the wall rock generally display higher iron contents, whereas most chlorites in the fault zone contain relatively more magnesium and silica. The "textural populations" of chlorites in the fault zone described earlier belong to the latter category and show overlapping compositions among them. This implies little or no change in fluid

TABLE 3

Microprobe analyses of amphibole

Sample no:	WALLROCK 161	WALLROCK 162	FAULT ZONE 1	FAULT ZONE 2	FAULT ZONE 3	FAULT ZONE 4	FAULT ZONE 6	FAULT ZONE 7	FAULT ZONE 8	FAULT ZONE 10	FAULT ZONE 12	FAULT ZONE 14	WALLROCK 163	WALLROCK 164	WALLROCK 165	WALLROCK 166
SiO_2	45.75	45.96	54.97	55.22	54.61	49.51	55.67	54.60	54.00	55.27	54.56	54.83	53.34	46.77	46.93	46.12
TiO_2	0.63	0.69	0.02	0.00	0.02	0.51	0.02	0.04	0.24	0.00	0.06	0.05	0.08	0.78	0.66	0.71
Al_2O_3	7.11	7.31	1.12	1.10	1.84	5.61	0.65	1.13	2.04	0.61	0.90	1.12	2.61	6.89	7.02	7.32
Cr_2O_3	0.08	0.10	0.02	0.13	0.12	0.03	0.03	0.02	0.09	0.10	0.10	0.12	0.09	0.14	0.05	0.11
FeO*	15.66	16.86	11.81	10.10	11.39	13.88	8.84	9.90	11.04	9.81	10.77	10.20	13.45	15.42	15.08	16.30
MnO	0.28	0.21	0.22	0.24	0.28	0.32	0.23	0.20	0.27	0.30	0.22	0.25	0.30	0.29	0.25	0.25
MgO	13.10	12.69	17.72	18.40	17.62	15.12	19.19	18.69	17.37	18.27	17.50	18.63	17.94	13.65	14.09	12.90
CaO	11.30	10.99	12.42	12.16	12.14	11.57	12.71	12.24	12.45	12.69	12.58	11.93	11.00	11.17	11.04	11.48
Na_2O	2.25	2.00	0.08	0.00	0.05	1.08	0.00	0.78	0.43	0.00	0.45	0.17	0.15	1.87	2.24	1.77
K_2O	1.09	0.96	0.27	0.07	0.31	0.76	0.07	0.14	0.30	0.11	0.17	0.15	0.13	0.98	0.94	1.16
Total	97.25	97.77	98.65	97.42	98.38	98.39	97.41	97.74	98.23	97.46	97.31	97.45	99.09	97.96	98.30	98.12

*Total iron as FeO.

Structural Formulae (based on 23 oxygens)

Si	6.794	6.761	7.700	7.743	7.640	7.076	7.809	7.690	7.629	7.846	7.791	7.681	7.328	6.825	6.811	6.778
Al	1.206	1.249	.185	.182	.304	.924	.108	.188	.340	.102	.152	.185	.423	1.175	1.189	1.222
Total	8.000	8.000	7.885	7.925	7.944	8.000	7.917	7.878	7.969	7.948	7.943	7.866	7.751	8.000	8.000	8.000
Al	.040	.029	---	---	---	.022	---	---	---	---	---	---	---	.011	.013	.047
Cr	.009	.012	.003	.015	.013	.004	.003	.002	.010	.011	.011	.013	.010	.016	.006	.013
Fe^{3+}	.566	.832	.611	.651	.692	.808	.435	.489	.401	.336	.237	.776	1.545	.773	.790	.667
Fe^{2+}	1.378	1.241	.682	.486	.617	.850	.547	.559	.903	.806	1.019	.314	0.000	1.108	1.040	1.335
Mg	2.901	2.784	3.702	3.848	3.676	3.223	4.014	3.926	3.660	3.847	3.727	3.892	3.676	2.971	3.050	2.828
Ti	.070	.076	.002	.000	.002	.055	.002	.004	.026	.000	.006	.005	.008	.086	.072	.078
Mn	.035	.026	---	---	---	.039	---	---	---	---	---	---	---	.036	.031	.031
M_1-M_3	4.999	5.000	5.000	5.000	5.000	5.001	5.000	5.000	5.000	5.000	5.000	5.000	5.239	4.990	4.989	4.952
Ca	1.798	1.732	1.864	1.827	1.819	1.772	1.910	1.847	1.884	1.920	1.925	1.790	1.619	1.746	1.716	1.808
Mn	---	---	.026	.029	.033	---	.027	.024	.032	.036	.027	.030	.035	---	---	---
Fe^{2+}	---	---	.090	.047	.023	---	.055	.098	---	.016	.030	.104	---	---	---	---
Na	.202	.268	.022	.000	.014	.228	.000	.031	.084	.000	.018	.046	.040	.254	.284	.192
M_4	2.000	2.000	2.002	1.903	1.889	2.000	1.992	2.000	2.000	1.972	2.000	1.970	1.694	2.000	2.000	2.000
Na	.446	.302	---	---	---	.071	---	.182	.034	---	.107	---	---	.275	.346	.312
K	.207	.180	.048	.013	.055	.139	.013	.025	.054	.020	.031	.027	.023	.182	.174	.218
A	.653	.482	.048	.013	.055	.210	.013	.207	.088	.020	.138	.027	.023	.457	.520	.530
Total	15.652	15.482	14.935	14.841	14.888	15.211	14.922	15.085	15.057	14.940	15.081	14.863	14.707	15.447	15.509	15.482

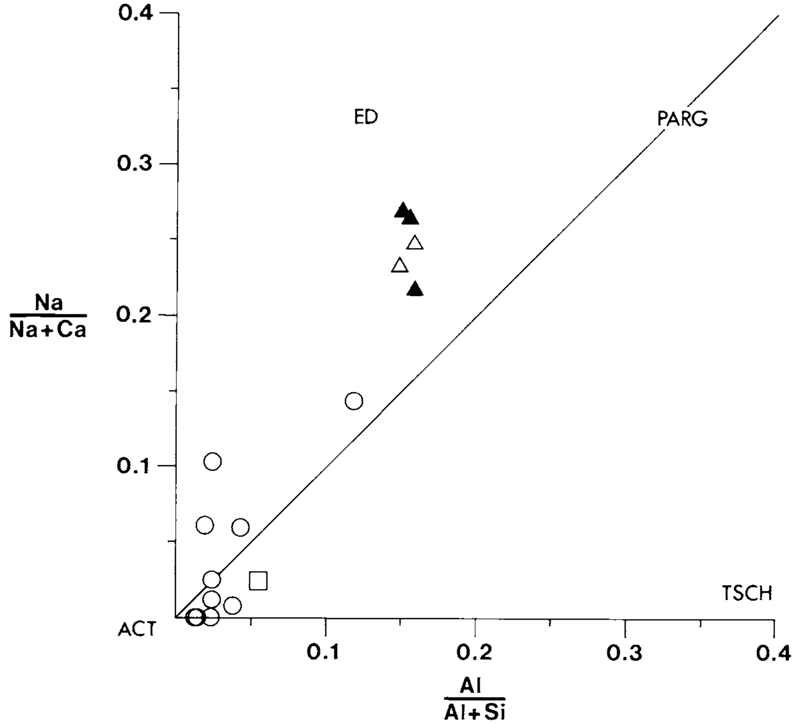

Fig. 9. Plot of Na/(Na + Ca) versus Al/(Al + Si) showing compositional variations of amphiboles. Solid triangles relatively unaltered amphiboles; open triangles weakly altered amphiboles; square moderately altered amphibole; circles highly altered amphiboles. ED = edenite, PARG = pargasite, TSCH = tschermakite, ACT = actinolite.

composition during rock alteration that produced various types of chlorites.

Prehnite.—Prehnite is mainly confined to the fault zone and is generally concentrated on plagioclase and amphibole porphyroclasts. Hence, its origin is likely linked with alteration processes related to cataclasis. Microprobe analyses of prehnite (table 7) indicate only minor compositional variations in terms of iron and aluminum content. One analyzed prehnite from the central portion of the fault zone contains low FeO (0.43 wt percent) but displays the highest Al_2O_3 and Na_2O contents observed. A progressive trend of over 1 wt percent increase in Al_2O_3 from the margin into the center of the fault zone is evident (see table 7). Prehnite occurring at the margin of the zone contains the highest magnesium.

White mica.—Fine-grained, prismatic flakes of white mica replacing plagioclase are common in the wall rock but not within chemically converted plagioclase in the fault zone. The white mica is, however, apparently present within cataclasite, perhaps as porphyroclastic materi-

TABLE 4

Microprobe analyses of sphene

Sample No:	Wallrock 161	Wallrock 162	Fault Zone 3	Fault Zone 4	Fault Zone 5	Fault Zone 8	Wall Rock 165
SiO_2	30.70	30.90	31.03	30.82	30.83	31.49	30.62
TiO_2	37.02	36.92	36.78	36.75	36.95	36.09	36.48
Al_2O_3	1.88	1.85	1.93	1.88	1.82	2.62	2.46
Cr_2O_3	0.03	0.10	0.12	0.10	0.11	0.00	0.06
FeO*	1.76	2.00	2.06	1.96	1.94	1.74	1.36
MgO	0.44	0.59	0.48	0.42	0.41	1.14	0.65
CaO	27.91	28.03	27.51	27.54	27.20	27.18	28.40
K_2O	0.04	0.10	0.03	0.09	0.07	0.08	0.10
Total	99.78	100.49	99.94	99.56	99.33	100.34	100.13
Structural Formulae (based on 20 oxygens)							
Si	4.027	4.029	4.059	4.051	4.092	4.083	3.999
Ti	3.652	3.621	3.619	3.632	3.678	3.520	3.583
Al	0.291	0.285	0.298	0.291	0.285	0.400	0.379
Cr	0.003	0.010	0.013	0.010	0.011	0.000	0.006
Fe	0.188	0.218	0.226	0.216	0.215	0.189	0.149
Mg	0.086	0.115	0.093	0.082	0.080	0.220	0.127
Ca	3.923	3.916	3.857	3.878	3.863	3.770	3.974
K	0.006	0.017	0.006	0.015	0.012	0.014	0.016

*Total Fe as FeO.

TABLE 5

Microprobe analyses of epidote
Sample 162(i)-epidote after plagioclase; 162(ii)-epidote after amphibole; 162(iii)-epidote after titanomagnetite

Sample No:	Wallrock 162 (i)	Wallrock 162 (ii)	Wallrock 162 (iii)	Fault Zone 1	Fault Zone 4	Fault Zone 6	Fault Zone 7	Fault Zone 8**
SiO_2	38.51	37.73	37.55	39.77	39.13	39.14	38.95	39.19
TiO_2	0.00	0.03	0.02	0.00	0.00	0.00	0.00	0.00
Al_2O_3	26.43	23.21	22.49	24.49	23.01	22.67	24.39	23.34
Cr_2O_3	0.05	0.08	0.06	0.07	0.05	0.09	0.05	0.04
FeO*	8.80	13.12	15.84	12.06	13.98	14.12	12.19	13.44
MnO	0.06	0.08	0.14	0.32	0.10	0.03	0.06	0.18
MgO	0.19	0.35	0.30	0.41	0.40	0.53	0.57	0.49
CaO	23.89	23.45	22.15	21.92	27.71	21.67	21.95	20.87
K_2O	0.02	0.06	0.05	0.13	0.17	0.17	0.02	0.07
Total	97.95	98.11	98.60	99.17	98.55	98.42	98.12	97.62
Structural Formulae (based on 25 oxygens)								
Si	6.112	6.156	6.153	6.312	6.321	6.335	6.235	6.352
Ti	—	0.034	0.002	—	—	—	—	—
Al	4.945	4.456	4.344	4.581	4.382	4.321	4.602	4.460
Cr	0.009	0.010	0.008	0.009	0.006	0.012	0.006	0.007
Fe	1.168	1.787	2.171	1.602	1.889	1.911	1.632	1.821
Mn	0.025	0.011	0.020	0.046	0.014	0.003	0.008	0.025
Mg	0.046	0.085	0.073	0.098	0.097	0.128	0.136	0.119
Ca	4.063	4.111	3.890	3.725	3.759	3.759	3.764	3.625
K	0.004	0.012	0.010	0.026	0.035	0.035	0.004	0.015

*Total Fe as FeO.
**Sample 8 contains 0.11 wt % Na_2O.

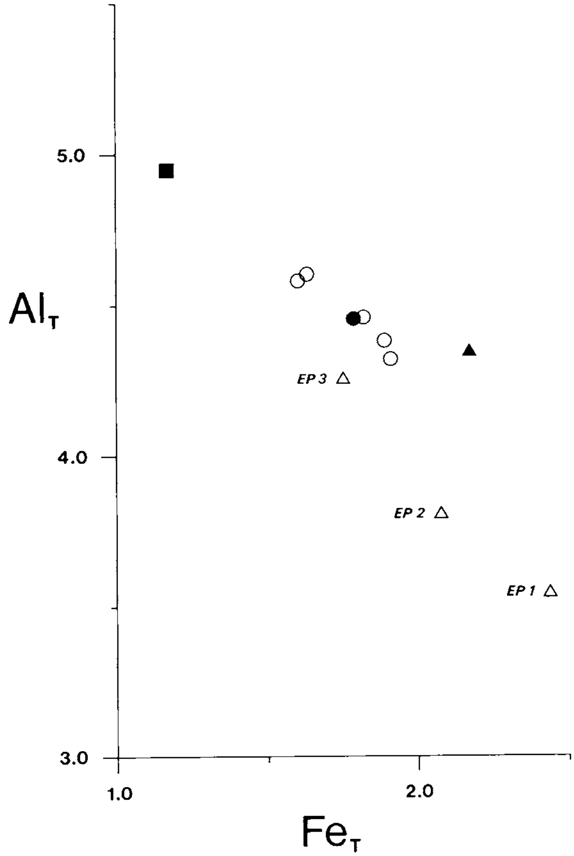

Fig. 10. Total Al versus total Fe plot showing compositional variations of epidote. Examples of epidote after plagioclase (solid square), amphibole (solid circle), and titano-magnetite (solid triangle) are from weakly altered monzodiorite (sample 162) outside the fault zone. All other analyses (open circles) are of epidote within the fault zone. The compositions of three successive generations of epidote (open triangles from Stone and Kamineni (1982) are shown for comparison.

al. The white mica may be an early alteration product of primary plagioclase in the Eye-Dashwa Lakes pluton which preceded, and was largely destroyed by, plagioclase alteration and mechanical breakdown related to cataclasis within the fault zone. Two types of white mica are identified by the chemical analyses (see table 8): samples 161 and 162 (in the fault hangingwall) and samples 164 and 165 (in the footwall). The former, containing significant amounts of iron and magnesium, may be classified as phengite according to Velde (1965).

Slip surfaces.—The vast majority of the ultrafine-grained crystals (>50 mm diam) within the slip surfaces display high birefringence under cross-polarized light suggesting that they are comprised mainly of

TABLE 6

Microprobe analyses of chlorite

Sample No:	Wall Rock 161	162	Fault Zone 1	2	4	5	6	7	8	14
SiO_2	29.32	27.52	27.56	29.27	29.21	29.84	27.54	30.25	30.36	29.24
TiO_2	0.10	0.13	0.06	0.05	0.09	0.08	0.03	0.05	0.03	0.05
Al_2O_3	18.27	18.80	18.26	17.86	18.23	18.66	18.25	18.08	18.08	17.39
Cr_2O_3	0.06	0.05	0.09	0.10	0.06	0.13	0.07	0.03	0.07	0.08
FeO*	22.28	22.14	22.35	23.80	19.31	20.45	23.35	18.30	19.43	18.85
MnO	0.42	0.43	0.31	0.40	0.30	0.31	0.28	0.31	0.26	0.26
MgO	21.10	19.60	19.30	19.94	21.82	21.93	19.02	23.65	22.36	22.27
CaO	0.05	0.06	0.11	0.10	0.08	0.20	0.01	0.29	0.29	0.12
K_2O	0.01	0.05	0.06	0.02	0.11	0.02	0.03	0.02	0.04	0.07
Total	91.61	88.78	88.10	91.54	89.21	91.62	88.58	90.98	90.92	88.33
Structural Formulae (based on 28 oxygens):										
Si	5.796	5.636	5.695	5.838	5.842	5.833	5.686	5.893	5.947	5.895
Ti	0.015	0.019	0.009	0.007	0.015	0.012	0.004	0.007	0.004	0.008
Al	4.255	4.538	4.448	4.198	4.299	4.300	4.441	4.152	4.147	4.142
Cr	0.009	0.009	0.014	0.015	0.009	0.021	0.011	0.005	0.010	0.008
Fe	3.684	3.792	3.864	3.970	3.229	3.344	4.031	2.981	3.183	3.190
Mn	0.070	0.074	0.055	0.067	0.050	0.051	0.049	0.051	0.042	0.045
Mg	6.216	5.983	5.946	5.929	6.506	6.391	5.854	6.868	6.530	6.689
Ca	0.011	0.013	0.025	0.021	0.021	0.041	0.003	0.060	0.060	0.025
K	0.003	0.014	0.016	0.005	0.029	0.004	0.008	0.006	0.011	0.005

*Total Fe as FeO.

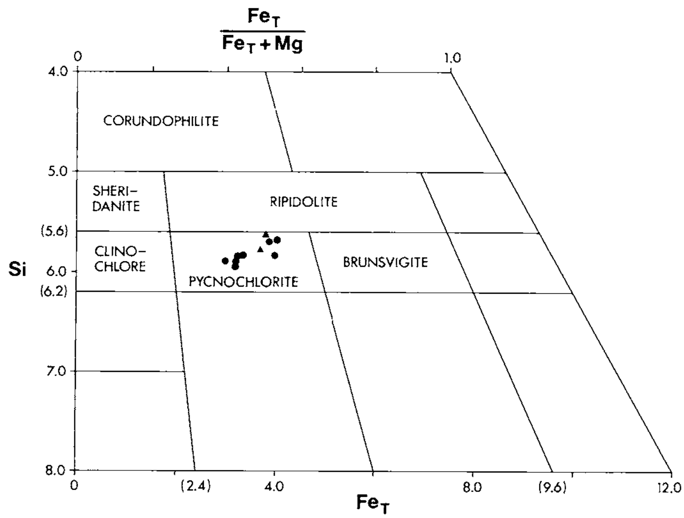

Fig. 11. $Fe_T/(Fe_T + Mg)$ versus Si plot (after Hey, 1954) showing compositional variation of chlorite. Triangles—chlorite from relatively unaltered monzodiorite, circles—chlorite from fault zone.

TABLE 7

Microprobe analyses of prehnite from the fault zone

Sample No:	1	3	6	8
SiO_2	43.63	42.88	43.55	43.22
TiO_2	0.03	0.04	0.04	0.01
Al_2O_3	23.03	23.59	23.89	24.18
Cr_2O_3	0.05	0.08	0.04	0.02
FeO*	1.19	0.98	1.11	0.43
MgO	0.41	0.30	0.20	0.33
CaO	26.74	27.31	27.25	26.81
Na_2O	0.10	0.00	0.12	0.29
K_2O	0.07	0.11	0.08	0.10
Total	94.95	95.29	96.28	95.39
Structural Formulae (based on 22 oxygens)				
Si	6.057	5.961	5.986	5.974
Ti	0.003	0.004	0.004	0.001
Al	3.769	3.865	3.871	3.934
Cr	0.006	0.009	0.005	0.002
Fe	0.138	0.114	0.127	0.050
Mg	0.085	0.062	0.041	0.068
Ca	3.978	4.069	4.014	3.971
Na	0.027	0.000	0.031	0.078
K	0.012	0.028	0.013	0.018

*Total Fe as FeO.

epidote. Microprobe analyses of slip surface material from sample 10 (table 9) indicate compositions in accord with epidote, chlorite, and white mica. However, the mineral analyses in table 9 illustrate some peculiar compositions (compare with tables 5, 6, and 8), likely owing to the effects of adjacent fine grains of other mineral species. For example, high CaO in chlorite and white mica may be attributed to interference

TABLE 8

Microprobe analyses of white mica from the wall rock

Sample No:	161	162	164	165
SiO_2	48.33	49.16	48.16	47.27
TiO_2	0.28	0.30	0.32	0.28
Al_2O_3	31.21	31.69	38.18	37.28
Cr_2O_3	0.03	0.05	0.00	0.03
FeO*	4.94	5.01	1.16	1.28
MnO	0.01	0.01	0.08	0.00
MgO	2.49	2.55	1.07	1.13
CaO	0.04	0.04	0.05	0.05
Na_2O	0.31	0.22	0.30	0.52
K_2O	7.61	7.36	7.63	7.86
Total	95.25	96.39	96.95	95.70
Structural Formulae (based on 22 oxygens)				
Si	6.429	6.445	6.155	6.145
Ti	0.029	0.030	0.031	0.028
Al	4.894	4.898	5.752	5.711
Cr	0.003	0.005	0.000	0.003
Fe	0.551	0.549	0.124	0.140
Mn	0.001	0.001	0.008	0.000
Mg	0.494	0.498	0.203	0.219
Ca	0.007	0.006	0.006	0.007
Na	0.080	0.055	0.075	0.130
K	1.292	1.230	1.245	1.303
Si:Al	1.314	1.316	1.070	1.076

*Total Fe as FeO.

TABLE 9

Microprobe analyses of fine-grained minerals from a slip plane (sample 10)

Mineral:	Chlorite	Epidote	White Mica
SiO_2	27.49	38.42	57.75
TiO_2	0.07	0.00	0.24
Al_2O_3	17.66	24.57	17.70
FeO*	16.55	13.50	3.20
MnO	0.22	0.06	0.05
MgO	18.55	1.50	3.58
CaO	2.15	21.55	2.25
Na_2O	0.00	0.00	0.35
K_2O	0.89	0.65	10.69
Total	83.58	100.25	95.81

*Total Fe as FeO.

from adjacent epidote grains. Other variations, such as high MgO in epidote and white mica, may be similarly regarded as interference from adjacent chlorite grains. Of particular interest are the noticeably high values of K_2O in all three minerals.

WHOLE ROCK COMPOSITIONS

Whole rock geochemical analyses presented in table 10 compare compositions of an average of 22 unaltered hornblende quartz monzodiorite samples ("A") from borehole ATK-6 with two similar wall rock monzodiorite samples (161, 162) and variably altered samples from the fault zone (1–14).

The major element concentrations of many unaltered and variably altered samples are similar except for notable variations in SiO_2 and Al_2O_3. The average monzodiorite and wall rock monzodiorite display comparable values, whereas one group comprising most fault zone samples is richer in SiO_2 (64–74 percent) and poorer in Al_2O_3 (10–14 percent). Another group of fault zone samples (7, 11, 12, 14) displays an opposite relationship, having lower SiO_2 (45–57 percent) and higher Al_2O_3 (16–18 percent). The latter group is generally richer in Fe_2O_3, MgO, and CaO, and poor in Na_2O. This group is composed of samples from slip surfaces rich in chlorite and epidote which have been subjected to later lower-temperature alteration either by prolonged groundwater activity or by fracture reactivation.

Rare-earth element concentrations in rocks of the fault zone are for the most part similar to those in the wall rock (table 10). All display subparallel, negative-sloping chondrite-normalized concentration patterns (fig. 10). The La/Yb ratios range between 39.17 to 83.25. Absolute concentrations as well as relative patterns of the altered and unaltered monzodiorite samples are comparable with those of the granite phase of the pluton (Kamineni, 1986a) with only minor differences. For example, the monzodiorite phase contains slightly more middle rare-earth element concentrations than the granite, producing patterns with slightly opposing convexity. Nevertheless, based upon a limited comparison with two analyzed samples of wall rock (161, 162), two geochemically distinct groups of fault zone rocks are evident. One group (samples 6, 8, 9, 10) is subtly depleted in all rare-earth elements. This group resembles the depleted patterns of altered granite relative to unaltered granite observed by Kamineni (1986a). Another group, however, (including samples 5, 7, 12, 13, 14) displays a slight relative enrichment in light rare-earth elements and a noticeable negative Dy anomaly, while the middle rare-earth elements and Yb remain comparable. Sample 11 is considered with this group but differs in its general enrichment in all rare-earth elements, particularly the middle rare-earth elements (see fig. 12B), and also contains the lowest SiO_2, and highest Al_2O_3, MgO, and CaO observed in the fault zone.

Samples from the two groups have similar textures comprising protocataclasite-breccia and cataclasite types. The rare-earth element

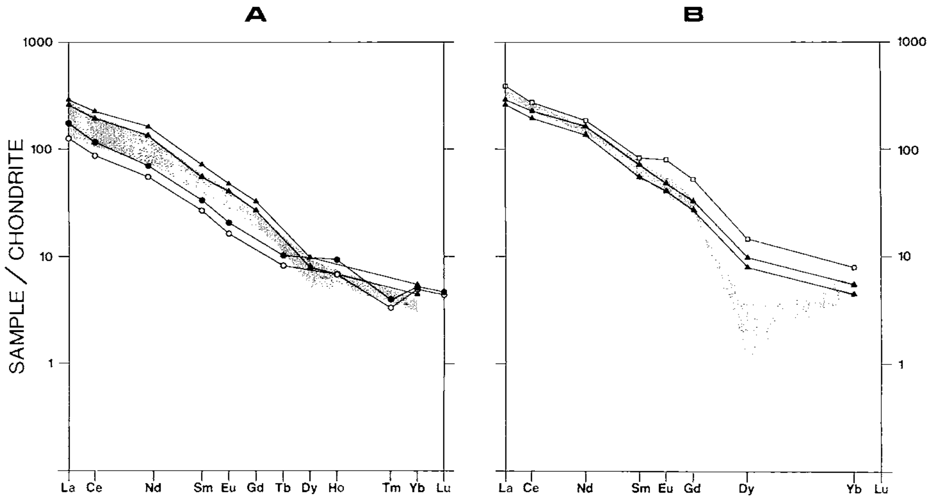

Fig. 12. Plot of chondrite-normalized rare-earth element concentrations versus atomic number for unaltered and altered hornblende quartz monzodiorite in the vicinity of the ATK-6 fault zone. (A) Unaltered wall rock concentrations (solid triangles; samples 161, 162) compared to altered fault rock concentration range (stippled), as well as to unaltered granite (solid circles, average of 20) and altered granite (open circles, average of 28) from Kamineni (1986a). Note the subparallel, but depleted patterns of altered rocks compared to unaltered rocks. (B) Unaltered wall rock concentrations (as in A) compared to altered fault rocks which are associated with lower-temperature alteration features (stippled; samples 5, 7, 12, 13, 14). Note the slight light rare earth enrichment and apparent negative Dy anomaly in the latter. Also shown are concentrations in sample 11 (squares) which are notably enriched in all rare earth elements, especially Eu and Gd.

differences of the second group reflect late alteration under low-temperature hydrothermal conditions relative to most ambient cataclasite and breccia temperature conditions operative in the proximity of open fractures. For example, samples 13 and 14, which are from the area of the lower slip surface dominated by hematite infilling, appear to have feldspars that recrystallized at temperatures lower than those within other slip surfaces. The area of the lower slip surface may have undergone rejuvenation subsequent to sealing. Sample 12 displays exceptional late-stage development of brown chlorite aggregates, carbonate, and prehnite and extreme replacement of titanomagnetite and sphene. Sample 7 contains a high Ba concentration in addition to this rare-earth element concentration pattern, apparently related to proximity with a late fracture containing barite and celestite. All the second group of fault rock samples also contain a slight enrichment in U, that is, up to two times the concentration apparent in the analyzed wall rock samples (table 10). Fracture environments subjected to lower-temperature alteration are the most enriched in uranium. Thorium, in general, shows little variation with reference to the wall rock except in some samples.

TABLE 10

Whole-rock geochemical analyses of an average unaltered monzodiorite (A; n = 22), wall rock monzodiorite (161, 162) and variably altered fault zone rocks (1–14) from borehole ATK-6

Sample No.:	A	stand. dev.	161	162	1	2	3	4	5	6	7	8	9	10	11	12	13	14
SiO_2	61.79	1.54	64.8	62.1	66.1	69.9	68.4	74.2	70.8	66.1	51.8	64.1	67.0	64.4	45.6	50.4	67.6	57.2
TiO_2	0.61	0.07	0.60	0.71	0.60	0.53	0.52	0.41	0.49	0.60	0.63	0.54	0.51	0.54	0.63	0.60	0.49	0.68
Al_2O_3	14.65	0.49	14.4	14.4	13.3	12.6	13.0	10.3	12.5	13.4	16.1	13.7	12.3	12.8	18.0	16.0	11.5	16.5
Fe_2O_3	4.52	0.38	1.4	1.6	2.1	0.9	1.2	1.3	1.1	1.8	5.4	2.8	1.3	2.2	5.8	n.r.	3.1	2.4
FeO	2.43	0.31	2.3	2.7	1.6	1.9	2.0	1.8	2.0	1.9	2.5	1.2	3.0	2.7	3.7	n.r.	1.5	1.5
MnO	0.07	0.01	0.07	0.08	0.06	0.06	0.05	0.05	0.06	0.06	0.07	0.05	0.07	0.07	0.10	0.06	0.05	0.04
MgO	2.45	0.27	2.56	2.48	2.82	2.43	2.45	2.42	2.14	2.88	4.13	2.24	4.08	3.96	5.68	3.05	2.67	3.47
CaO	4.59	0.75	3.24	4.95	3.45	2.76	3.40	2.63	2.63	3.35	5.89	5.37	2.17	3.68	8.91	8.32	4.37	2.44
Na_2O	4.51	0.25	4.43	4.11	4.19	4.10	3.30	2.31	4.15	3.07	1.03	2.25	2.46	1.76	1.18	1.23	0.20	4.16
K_2O	4.14	0.28	4.28	4.07	4.00	3.59	4.14	3.22	3.64	4.89	7.27	5.02	3.51	4.17	4.19	6.75	5.52	6.13
H_2O_T	n.d.	---	0.9	0.7	1.1	0.9	1.3	1.3	1.0	1.3	2.9	1.8	2.2	2.6	3.9	n.r.	1.6	2.4
CO_{2T}	n.d.	---	0.0	0.2	0.4	0.2	0.8	0.2	0.3	1.3	1.2	1.8	0.5	1.2	1.2	0.4	0.7	1.9
P_2O_5	0.41	0.12	0.39	0.48	0.37	0.30	0.33	0.27	0.29	0.39	0.42	0.36	0.31	0.36	0.43	0.47	0.29	0.37
S	0.13	0.03	0.09	0.09	0.13	0.05	0.00	0.11	0.12	0.00	0.28	0.16	0.03	0.15	0.15	1.09	0.05	0.07
Total	100.30		99.46	98.67	100.22	100.22	100.89	100.52	101.22	101.04	99.62	101.39	99.44	100.59	99.47	88.37	99.64	99.26
Trace elements (ppm)																		
Ba	1826	169.72	1900	1700	1500	1500	1100	1300	1800	2200	1700	1000	1300	1300	1300	2000	1700	1900
Rb	86	15.24	86	75	98	89	74	88	120	120	95	120	95	120	81	150	140	150
Sr	1756	294.59	1200	2100	960	820	1300	1000	800	1400	2600	2600	910	1600	4500	3900	2600	1100
U	3.4	0.86	2.5	2.8	3.4	3.5	3.8	2.9	4.0	3.3	6.6	2.8	3.7	4.6	8.0	7.0	6.5	7.7
Th	15.5	4.53	16.8	15.0	15.2	15.0	18.2	15.5	17.0	14.5	18.0	17.0	14.0	15.6	12.1	9.3	14.9	14.0
Rare earth elements (ppm)																		
La			86	96	73	71	94	79	110	90	105	72	43	66	130	110	120	120
Ce			170	200	160	150	170	150	200	180	205	140	92	130	240	210	220	240
Nd			81	97	75	70	76	66	84	81	98	65	45	63	110	91	95	100
Sm			10	13	11	9.4	9.5	8.4	11	11	13.5	8.0	6.8	9.1	15	9.4	11	14
Eu			2.8	3.3	2.6	2.3	2.5	2.3	2.5	2.9	4.0	2.5	1.9	2.8	5.5	3.1	3.1	3.8
Gd			6.7	8.1	6.5	5.8	5.9	5.2	7.0	6.6	9.0	5.5	4.5	6.3	13	6.2	6.4	8.7
Dy			2.6	3.2	2.9	2.4	1.8	1.9	3.6	2.5	3.6	1.7	2.4	3.1	4.7	0.6	1.2	3.6
Yb			0.9	1.1	0.8	0.7	0.7	0.7	1.7	0.8	1.0	0.8	0.6	0.8	1.6	0.8	0.9	1.3
Y			16	18	15	13	13	11	20	14	18	13	11	14	29	16	14	20

AMBIENT P-T CONDITIONS OF DEFORMATION

The fault zone contains a variety of secondary minerals useful for assessing P-T conditions of deformation, that is, albite, chlorite, actinolite, epidote, and prehnite. Reference to the stability of these minerals suggests that they have overlapping P-T fields. The most diagnostic and common assemblage is epidote + chlorite + actinolite + quartz, which belongs to the greenschist facies (Liou, Kuniyoshi, and Ito, 1974; Moody, Meyer, and Jenkins, 1983) and has an upper limit of 475°C at 2 kb (Liou, Kuniyoshi, and Ito, 1974). Since none of the high-temperature precursors of secondary breakdown products, such as hornblende, of this assemblage are found in the fault zone, it can be inferred that the highest temperature during cataclasis was definitely below 475°C. The "peak" condition of brittle deformation, which produced greenschist facies assemblages, was preceded and/or followed by sub-greenschist conditions forming the assemblage prehnite-chlorite-actinolite. Schiffman and Liou (1980) suggest that the mineral assemblage prehnite-chlorite-actinolite (+ quartz + albite) is stable between 2.5 to 5 kb at temperatures of 325° to 375°C, respectively, and is intermediate between the sub-greenschist assemblage pumpeyllite–chlorite–actinolite and greenschist assemblage clinozoisite–chlorite–actinolite (fig. 13).

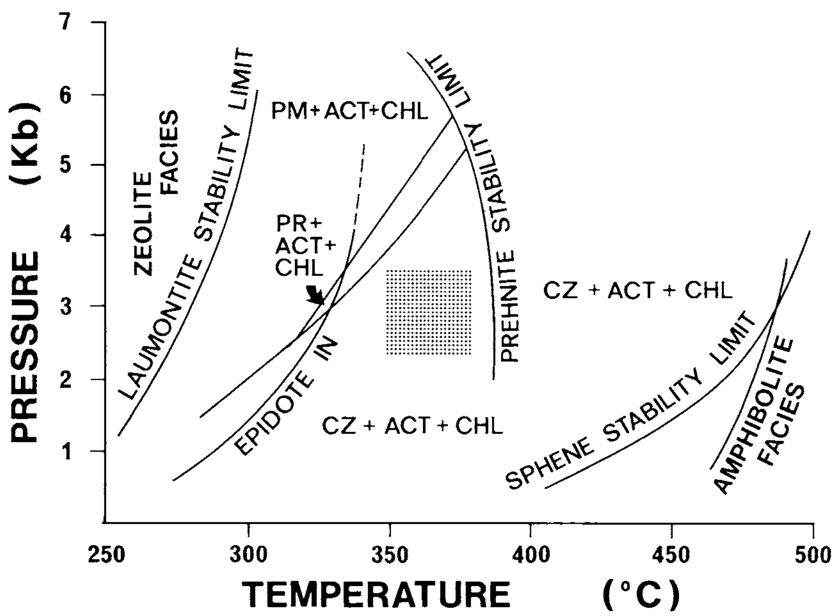

Fig. 13. Pressure-temperature plot showing stability fields of index minerals and assemblages, and the estimated P-T field (stippled) in which faulting occurred. Prehnite and laumontite stability limits are from Liou (1971a,b); epidote and sphene stability limits are from Moody, Meyer and Jenkins (1983); greenschist-amphibolite facies boundary is from Liou Kunoyoshi and Ito (1974). Phase relations among ACT (actinolite), CHL (chlorite), CZ (clinozoisite), PM (pumpellyite) are from Schiffman and Liou (1980).

Epidote or pumpeyllite may be formed with the prehnite–chlorite–actinolite assemblage (Schiffman and Liou, 1980). However, pumpeyllite appears to be present in high-pressure terrains (Seki, 1966) but not in areas of relatively high geothermal gradients (Kuniyoshi and Liou, 1976). The absence of pumpellyite in the fault zone thus constrains the upper pressure limitation, which cannot have exceeded 3.5 kb.

Based on the above arguments ranges in temperature of 325° to 400°C and pressure of 2.5 to 3.5 kb can be assigned for the ambient conditions of alteration and cataclasis in the fault zone. A field encompassing these P-T conditions is shown in figure 13. These P-T conditions correspond to a geothermal gradient of about 35°C/km.

The temperature of alteration and microfracturing inferred above from mineral stability is corroborated by an independent estimate based on the partitioning of the albite component of feldspar between coexisting plagioclase and microcline (see table 11). This method is suggested by Whitney and Stormer (1977) and Ferry (1978) from the microcline-low albite mixing parameters of Bachinski and Muller (1971). Calculated temperatures obtained from eight coexisting feldspar pairs around the fault zone range between 412° and 297°C, with a mean temperature of 366°C. The variability in these calculated temperatures is possibly related to local conditions within the fault zone during alteration and cataclasis. For example, feldspar pairs in samples 1 and 2, which are located in altered and fractured monzodiorite within 2 m above the upper slip surface (that is, marginal to the fault zone), yield the highest temperature estimates (around 400°–410°C). The feldspar pair of sample 6, taken from fractured and altered monzodiorite between the two upper slip planes, also gives a similarly high temperature estimate (around 400°C). Feldspar pairs in four other samples come from epidote- and chlorite-rich slip planes or from brecciated rock within 0.5 m of a slip surfaces and correspond to more uniform temperature estimates ranging between 333° to 388°C, with an average of 353°C.

TABLE 11

Radiometric ages of some mineral and whole-rock samples from the Eye-Dashwa Lakes pluton

Type of material	Method	Age (Ma)	Reference
1. Hornblende from unaltered monzodiorite from the eastern pluton rim.	K-Ar	2658 ± 67	Kamineni and Stone (1983)
2. Hornblende from granite from a fault zone within the pluton rim.	K-Ar	2472 ± 71	Kamineni and Stone (1983)
3. Average whole rock isochron age of granodiorite from the pluton rim (n = 16; samples recovered from 1 km depth in borehole (ATK-1).	Rb-Sr	2632 ± 29	Peterman and others (1985)
4. Average of epidotized fault rock and epidote separates (N = 10; collected from various fault and fracture zones in borehole ATK-1).	Rb-Sr	2308 ± 155	Peterman and others (1985)

These may be regarded as more directly reflecting the temperature conditions during alteration and cataclasis, while the former feldspar pairs reflect the influence of higher temperature phases which are incompletely equilibrated by the retrogression observed within or nearer the slip planes themselves. Notably, feldspar pairs from samples 7 and 8 both yield temperatures around 335°C, near the lower extreme of the observed range, and are spatially associated with late barite-celestite and an open fracture respectively. In contrast, the feldspar pair in sample 14, taken from the lower slip surface, which is notably rich in hematite and hydrous iron oxides and forms part of a relatively "open" fracture system, yields the lowest temperature estimate (297°C). These relationships suggest a relatively continuous spectrum of feldspar recrystallization through lower-temperature rock-water interactions resulting from either prolonged activity following major cataclasis or by later independent hydrothermal activity, which is reflected in extreme K-rich compositions of K-feldspar.

AGE OF CATACLASIS

Although direct dating of the cataclastic zone described here is not available at present, some inferences as to its age can be deduced from published radiometric data from the Eye-Dashwa Lakes pluton (see table 11). The samples listed in table 11 were collected from the eastern margin of the pluton ("Grid Area" of fig. 1) located about 4 km away from the fault zone of the present study. The fault material dated is quite similar in mineralogical and textural characteristics to the cataclasites described here. It may be reasonable to assume that factors governing the processes of alteration in the two faulted areas of the pluton were similar (producing similar secondary mineral compositions) and acted contemporaneously.

Kamineni and Stone (1983) documented early emplacement of aplite dikes (2655 ± 31 Ma; K-Ar muscovite) followed by faulting at 2472 Ma (based on K-Ar hornblende from fault zone). However, subsequent work by Peterman and others (1985) suggests much younger fault activity around 2308 Ma. Uncertainty surrounds the precise longevity and reactivation periods of certain faults and fractures, and it is not clear whether the fault history involved "continuous," episodic, or single and independent periods of activity through the early Proterozoic. From table 11, it is evident that, regardless of the radiometric dating technique used, closure ages of the fault rock are 200 to 300 Ma younger than its unfaulted counterpart. In summary, it can be concluded that the pluton crystallized during the Kenoran Orogeny and was later affected by protracted faulting during late Archean and/or early Proterozoic times.

GEOPHYSICAL CHARACTERISTICS OF THE FAULT ZONE

Borehole geophysical surveys reflect well certain diagnostic features of rock alteration, intense fracturing, and cataclasis characteristic of the deep fault zone in borehole ATK-6. Relative to the monzodioritic wallrock, the fault zone is characterized by significant decreases in magnetic susceptibility, resistivity, and acoustic velocity, and increases in spontaneous potential, natural gamma, and acoustic amplitude.

A natural gamma survey displays a weak but broad radioelement enrichment centered about the fault zone, possibly influencing a region at least 30 m wide, normal to the zone, producing up to 220 cps compared to 130 to 150 cps from the monzodioritic wallrock distant to the zone. Geochemical analyses (see table 10) show that U is modestly enriched in some fault zone rocks while Th concentrations remain comparable to those in the wallrock. The general lack of clay minerals in the fault zone, which could accommodate K in their structure, suggests that ^{40}K is not a significant source of the observed radioelement enrichment. A weak but broad radioelement enrichment around the fault zone is similarly reflected by a borehole natural gamma log (J. Hayles, personal commun, 1985). It is tentatively concluded that ^{238,235}U, and not ^{232}Th, accounts for this slight enrichment.

A nearly total decline in magnetic susceptibility values is observed in the fault zone from moderate values of 2000 to 7000 × 10^6 SI in the monzodioritic wallrock. This appears to reflect a total breakdown of titanomagnetite observed petrographically, as described earlier, since it is the only primary mineral in the monzodiorite to influence strongly its magnetic behavior.

Significant broad decreases in resistivity values of three- to four-fold magnitude are observed in the fault zone relative to the wallrock, coinciding with an anomalous increase (up to 1700 millivolts) in spontaneous potential. These suggest that the altered and fractured rocks of the fault zone are electrically conductive: low resistance and/or enhanced conductivity may be explained in part by large chlorite concentrations along interconnected comminution zones and fractures, and by the fracture system itself possessing anisotropy (see fig. 5).

Slower acoustic velocity and irregular but relatively high acoustic amplitude in the fault zone suggest that the rocks are less dense and/or more fractured, with discontinuities that may delay acoustic travel time and enhance acoustic amplitude. These conclusions are corroborated by preliminary calibrations of effective rock density, which indicate a significant decrease in apparent density of as much as 0.05 g/cm^3 between wallrock monzodiorite and faulted, altered monzodiorite. Transgranular fracturing, which generates cataclastic rocks, involves volume dilatation, and this accounts for both the diminished resistivity and acoustic velocity.

DISCUSSION AND CONCLUSIONS

The fault cutting hornblende quartz mozodiorite at 1.1 km depth in borehole ATK-6 is a steep, west-southwesterly dipping zone of cataclasis associated with mid-greenschist facies retrograde alteration. The geometric relationship of similarly steep secondary fractures, which are inclined at small angle to the major slip surfaces (up to 25°), suggests a mainly strike-slip component of shear, possibly sinistral, across the fault zone.

The assemblage epidote-chlorite-actinolite-albite ± prehnite in part forms minor alterations away from the fault but constitutes the major neomineralized volume of the fault zone. A systematic variation in hornblende and plagioclase composition is evident within 10 to 12 m normal to the fault. An interrelationship is suggested with progressive alteration of primary amphibole (edenite or edenitic hornblende) and plagioclase (calcic oligoclase) such that coexisting species become ferrian magnesio-hornblende and sodic oligoclase surrounding the fault, ferri-tremolitic hornblende or ferrian tremolite and albite adjacent to parts of the fault, and actinolite and purer albite within the fault. Similar trends in the chemical conversion of hornblende to progressively more Mg-rich and Fe-poor (actinolitic) compositions are observed in other cataclastic rocks (for example, Brodie and Rutter, 1985; Kamineni, 1986b) as well as in brittle-to-ductile shear zones (Simpson, 1986). Brodie and Rutter (1985) demonstrate that the cation ratios Na/(Na + Ca) and Al/(Al + Si) in the molecular structure of hornblende may be sensitive to pressure and postulate higher and lower pressure amphibole metamorphic compositional series on this basis.

Bulk rock and mineralogical variations suggest that a large proportion of the elements released during alteration of the wall rock have been reconstituted within the fault zone. The obliteration of primary titanomagnetite by oxidation to form hematite in the fault zone is well reflected by low magnetic susceptibility. The presence of epidote clasts and crenulated actinolite clasts within cataclasite suggests that products of advanced alteration preceded some fault movement(s). The presence of cataclasite fragments within cataclasite infers conditions of transient cataclasis and episodic mechanical reworking during fault history, likely related to stick-slip movements. Borehole measurements of resistivity, spontaneous potential, acoustic velocity and amplitude made with geophysical probes reflect the fractured nature of the fault zone and its relative electrical conductivity and hydraulic permeability with respect to the wall rock.

At its time of formation, the fault zone is envisaged as a zone of relatively high strain in a heterogeneously deforming brittle environment. Hydraulic fracturing within the evolving fault zone initially enhanced alteration patterns within and surround the zone with the erection of hydrothermal/chemical gradients. Active processes within the fault zone likely included transgranular fracturing, grain boundary slip, and intergranular diffusion. The introduction of an aqueous fluid may have induced pressure solution and lowered the effective temperature for grain boundary diffusion within the evolving system. While pressure solution may be inhibited for high strain rates in an aseismic fault for grain sizes around 100 mm, it may become important at smaller grain sizes around 10 mm, even well above the "brittle-ductile mechanical transition" (compare Sibson, 1977). Since areas of cataclasite and ultracataclasite display epidote and albite grain sizes in the order of 15 to 30 mm, and ranging between 5 to 100 mm, it appears feasible that pressure solution played a large role in fault deformation. Chemical gradients were established that removed Ca, Al, Fe, and Si from the primary mineral assemblage and reconstituted these, at least in large part, within the neocrystallized assemblage of the fault zone. Reconstitution of elements may have been proximal in the case of incipient comminution zones (that is, grain or thin-section scale) and more distal in the case of major slip surfaces (that is, meter-scale or larger). Radioelements and water appear to have migrated into the fault zone, where conditions of oxidation (high oxygen fugacity) were conducive to the complete chemical breakdown of titanomagnetite and the crystallization of hematite and epidote. The lack of carbonate as a secondary mineral (except in areas of post-cataclasis alteration) and as a fracture filling in the fault zone also reflects relatively high oxygen fugacity.

Faulting likely occurred during the late Archean and/or early Proterozoic (about 2.31–2.47 Ga). Although the timing of fault development is not well constrained, and the crust may have subsequently experienced both uplift and burial, the pressure estimate of brittle fracturing is consistent with emplacement conditions. Kamineni and Stone (1983) conclude from several lines of evidence that the present erosional surface of the Eye-Dashwa Lakes pluton represents syn-Kenoran (about 2.63–2.67 Ga) intrusion levels in the surrounding rocks corresponding to prevailing greenschist and amphibolite facies metamorphic conditions. The presence of sillimanite and andalusite and the absence of kyanite in local surrounding metapelitic rocks indicate that the pressure of metamorphism did not exceed about 3 kb (Holdaway, 1971). Pressures around 3.0 to 3.5 kb and temperatures around 325° to 400°C are suggested for brittle fault conditions by mineral assemblage stability relations. Temperature estimates are corroborated by application of two-feldspar geothermometry, particularly by feldspar pairs within or around slip surfaces (ranging between 333°–388°C). The inferred depth of burial at this time, about 10 km, was probably very near the brittle-ductile transition, since semi-ductile features, such as prophyroclast elongation parallel to slip surface walls, are locally evident. Post-faulting uplift of the area by as much as 8 km by Ordovician time (about 2.3–0.5 Ga) is suggested by fission-track studies of apatite (Peterman and others, 1985). This indeed coincides with the present encountered level of 1 km for the fault zone and infers Proterozoic and/or early Paleozoic crustal instability but relative stability with a low rate of uplift and erosion since then.

ACKNOWLEDGMENTS

The authors are most grateful for borehole lithological and fracture data provided by J. J. B. Dugal, geophysical logs and comments obtained from J. Hayles and G. M. Reeves, borehole television data from J. S. O. Lau and L. F. Auger, and computerized drill core information and plots provided by B. N. Dukkipati. M. Bonardi is thanked for his help and supervision on the electron microprobe. This paper benefited greatly from reviews of original drafts by R. Kerrich, R. Kretz, P. A. Brown, the journal referees, and the editors.

References

Bachinski, S. W., and Muller, G., 1971, Experimental determinations of the microcline-low albite solvus: Jour. Petrology, v. 12, p. 329–356.

Brodie, K. H., and Rutter, E. H., 1985, On the relationship between deformation and metamorphism, with special reference to the behaviour of basic rocks, *in* Thompson, A. B., and Rubie, D. C., eds., Metamorphic reactions—kinetics, textures and deformation: New York, N.Y., Springer-Verlag, p. 138–179.

Brown, P. A., Kamineni, D. C., Stone, D., and Thivierge, R. H., 1980, General geology of the Eye-Dashwa Lakes pluton, Atikokan, northwestern Ontario, *In* Current Research, Pt. A: Canada Geol. Survey Paper 80-1A, p. 379–384.

Brown, P. A., and Rey, N., 1985, Fracture characteristics within a 4 km^2 region of the Eye-Dashwa pluton. In the geoscience program—proceedings of the seventeenth information meeting of the Nuclear Fuel Waste Management Program: Atomic Energy of Canada Ltd., Tech. Record 299, v. II, p. 477–490.

Chester, F. M., Friedman, M., and Logan, J. M., 1985, Foliated cataclasites: Tectonophysics, v. 111, p. 139–146.

Fenwick, W. G., 1976, Geology of the Finlayson Lake area, District of Rainy River: Ontario Div. Mines, Geosci. Rept. 145, 86 p.

Ferry, J. M., 1978, Fluid interaction between granite and sediment during metamorphism, south-central Maine: Am. Jour. Sci., v. 278, p. 1025–1056.

Griffin, W. L., and Heier, K. S., 1973, Petrological implications of some corona structures: Lithos, v. 6, p. 315–335.

Hey, M. H., 1954, A new review of the chlorites: Mineralog. Mag., v. 30, p. 277–292.

Higgins, M. W., 1971, Cataclastic rocks: U.S. Geol. Survey, Prof. Paper 687, 97 p.

Holdaway, M. J., 1971, Stability of andalusite and the aluminum silicate phase diagram: Am. Jour. Sci., v. 271, p. 97–113.

Holdaway, M. J., 1972, Thermal stability of Al-Fe epidote as a function of fO_2 and Fe content: Contr. Mineralogy Petrology, v. 37, p. 307–340.

Holloway, A. L., 1985, Sonar profiling in lakes near the Atikokan research area, Ontario. In the Geoscience program—proceedings of the seventeenth information meeting of the Nuclear Fuel Waste Management Program: Atomic Energy of Canada Ltd., Tech. Record 299, v. II, p. 622–633.

House, W. M., and Gray, D. R., 1982, Cataclasites along the Saltville thrust, U.S.A., and their implications for thrust-sheet emplacement: Jour. Structural Geology, v. 4, p. 257–269.

Hunt, J. A., and Kerrick, D. M., 1977, The stability of sphene; experimental redetermination and geologic implications: Geochim. et Cosmochim. Acta, v. 41, p. 279–288.

Kamineni, D. C., 1986a, The distribution of uranium, thorium and rare earth elements in the Eye-Dashwa Lakes pluton—a study of some analogue elements: Chem. Geology, v. 55, p. 361–373.

———— 1986b, A petrochemical study of calcic amphiboles from the East Bull Lake anorthosite-gabbro layered complex, District of Algoma, Ontario: Contr. Mineralogy Petrology, v. 93, p. 471–481.

Kamineni, D. C., and Brown, P. A., 1981, A preliminary report on the petrology and fracture fillings of the Eye-Dashwa Lakes pluton, Atikokan, northwestern Ontario: Atomic Energy of Canada Ltd., Tech. Record 123, 37 p.

Kamineni, D. C., and Stone, D., 1983, The ages of fractures in the Eye-Dashwa pluton, Atikokan, Canada: Contr. Mineralogy Petrology, v. 83, p. 237–246.

Kuniyoshi, S., and Liou, J. G., 1976, Contact metamorphism of the Karmutsen volcanics, Vancouver Island, British Columbia: Jour. Petrology, v. 17, p. 73-99.

Leake, B. E., 1978, Nomenclature of amphiboles: Canadian Mineralogist, v. 16, p. 501–520.

Liou, J. G., 1971a, P-T stabilities of laumontite, wairakite, lawsonite and related minerals in the system $CaAl_2Si_2O_8$-SiO_2-H_2O: Jour. Petrology, v. 12, p. 379–411.

———— 1971b, Synthesis and stability relations of prehnite, $Ca_2Al_2Si_3O_{10}(OH)_2$: Am. Mineralogist, v. 56, p. 507–531.

Liou, J. G., Kuniyoshi, S., and Ito, K., 1974, Experimental studies of the phase relations between greenschist and amphibolite in a basaltic system: Am. Jour. Sci., v. 274, p. 613–632.

Mitra, G., 1984, Brittle to ductile transition due to large strains along the White Rock Thrust, Wind River Mountains, Wyoming: Jour. Structural Geology, v. 6, p. 51–62.
Moody, J. B., Meyer, D., and Jenkins, J. E., 1983, Experimental characterization of the greenschist/amphibolite boundary in mafic systems: Am. Jour. Sci., v. 283, p. 48–92.
Peterman, Z. E., Goldich, S. S., Doe, B. R., Naeser, C. W., Rosholt, J. N., Zartman, R. E., and Kamineni, D. C., 1985, Isotopic studies of core samples from the Eye-Dashwa Lakes pluton, Atikokan, Ontario, *in* The geoscience program—proceedings of the seventeenth information meeting of the Nuclear Fuel Waste Management Program: Atomic Energy of Canada Ltd., Tech. Record 299, v. II, p. 642–643.
Rock, N. M. S., and Leake, B. E., 1984, The International Mineralogical Association amphibole nomenclature scheme: computerization and its consequences: Mineralog. Mag., v. 48, p. 211–227.
Schiffman, P., and Liou, J. G., 1980, Synthesis and stability relations of Mg-Al pumpellyite, $Ca_4Al_5MgSi_6O_{21}(OH)_7$: Jour. Petrology, v. 21, p. 441–474.
Schwerdtner, W. M., 1976, Lithology and structure of the Irene-Eltrut Lakes granitic complex between Akikokan and Ignace—a progress report, in 1976 Geotraverse Conference Proc.: Ontario, Univ. of Toronto, p. 22–27.
Schwerdtner, W. M., Stone, D., Osadetz, K., Morgan, J., and Stott, G. M., 1979, Granitoid complexes and the Archean tectonic record in the southern part of northwestern Ontario: Canadian Jour. Earth Sci., v. 16, p. 1965–1977.
Seki, Y., 1966, Pumpellyite-bearing mineral assemblages and type of metamorphism: Japanese Assoc. of Mineralogists, Petrologists, and Econ. Geologists Jour., v. 55, p. 105–112.
Shklanka, R., 1972, Geology of the Steep Rock Lake area, District of Rainy River: Ontario Dept. Mines and Northern Affairs, Geol. Rept. 93, 114 p.
Sibson, R. H., 1977, Fault rocks and fault mechanics: Geol. Soc. London Jour., v. 133, p. 191–213.
———— 1986, Brecciation processes in fault zones: inferences from earthquake rupturing: Pure and Appl. Geophysics, v. 124, p. 159–175.
Simpson, Carol, 1986. Fabric development in brittle-to-ductile shear zones: Pure and Appl. Geophysics, v. 124, p. 269–288.
Sinha, A. K., Collett, L. S., and Bazinet, R., 1985, Geophysical analysis of the new intrablock grid at Atikokan, *In* The geoscience program—proceedings of the seventeenth information meeting of the Nuclear Fuel Waste Management Program: Atomic Energy of Canada Ltd., Tech. Record 299, v. I, p. 78–97.
Stel, H., 1986. The effect of cyclic operation of brittle and ductile deformation on the metamorphic assemblage in cataclasites and mylonites: Pure and Appl. Geophysics, v. 124, p. 289–307.
Stone, D., 1983, Morphology of 'isolated' epidote faults in the Eye-Dashwa pluton, Atikokan, Ontario (abs.), *in* Schwerdtner, W. M., ed., Report on the second meeting of the Canadian Tectonics Group held on 23–24 October 1982 at Gravenhurst, near Toronto: Jour. Structure Geology, v. 5, p. 553.
———— 1985, Analysis of faults in the Atikokan grid area. In the geoscience program—proceedings of the seventeenth information meeting of the Nuclear Fuel Waste Management Program: Atomic Energy of Canada Ltd., Tech. Record 299, v. I, p. 98–112.
———— 1986, Geology of the Atikokan area, northwestern Ontario: Canada, Geol. Survey, Open File Map 1221.
Stone, D., and Kamineni, D. C., 1982, Fractures and fracture infillings of the Eye-Dashwa Lakes pluton, Atikokan, Ontario: Canadian Jour. Earth Sci., v. 19, p. 789–803.
Streckeisen, A., 1976, To each plutonic rock its proper name: Earth Sci. Rev., v. 12, p. 1–33.
Velde, B., 1965, Phengite micas: Synthesis, stability and natural occurrence: Am. Jour. Sci., v. 263, p. 886–913.
Whitney, J. A., and Stormer, J. C., Jr., 1977, The distribution of $NaAlSi_3O_8$ between coexisting microcline and plagioclase and its effect on geothermometric calculations: Am. Mineralogist, v. 62, p. 687–691.
Wise, D. U., Dunn, D. E., Engelder, J. T., Geiser, P. A., Hatcher, R. D., Kish, S. A., Odom, A. L., and Schamel, S., 1984, Fault-related rocks: suggestions for terminology: Geology, v. 12, p. 391–394.